THE JOURNAL OF BIOLOGICAL CHEMISTRY VOL. 290, NO. 45, pp. 27067–27089, November 6, 2015

Histone Deacetylase 3 Coordinates Deacetylase-independent Epigenetic Silencing of Transforming Growth Factor-β1 (TGF-β1) to Orchestrate Second Heart Field Development*

Received for publication, August 14, 2015, and in revised form, September 21, 2015 Published, JBC Papers in Press, September 29, 2015, DOI 10.1074/jbc.M115.684753

Sara L. Lewandowski, Harish P. Janardhan, and Chinmay M. Trivedi[1]

From the Division of Cardiovascular Medicine, Department of Medicine, University of Massachusetts Medical School, Worcester, Massachusetts 01605

Background: Histone-modifying genes play critical roles in the pathogenesis of human congenital heart disease.
Results: HDAC3 recruits PRC2 complex to mediate epigenetic silencing of TGF-β1 in a deacetylase-independent manner within second heart field progenitor cells.
Conclusion: HDAC3-mediated epigenetic silencing of TGF-β1 is required for normal heart development.
Significance: This is the first report of HDAC-mediated epigenetic regulation of second heart field development.

About two-thirds of human congenital heart disease involves second heart field-derived structures. Histone-modifying enzymes, histone deacetylases (HDACs), regulate the epigenome; however, their functions within the second heart field remain elusive. Here we demonstrate that histone deacetylase 3 (HDAC3) orchestrates epigenetic silencing of *Tgf-β1*, a causative factor in congenital heart disease pathogenesis, in a deacetylase-independent manner to regulate development of second heart field-derived structures. In murine embryos lacking HDAC3 in the second heart field, increased TGF-β1 bioavailability is associated with ascending aortic dilatation, outflow tract malrotation, overriding aorta, double outlet right ventricle, aberrant semilunar valve development, bicuspid aortic valve, ventricular septal defects, and embryonic lethality. Activation of TGF-β signaling causes aberrant endothelial-to-mesenchymal transition and altered extracellular matrix homeostasis in HDAC3-null outflow tracts and semilunar valves, and pharmacological inhibition of TGF-β rescues these defects. HDAC3 recruits components of the PRC2 complex, methyltransferase EZH2, EED, and SUZ12, to the NCOR complex to enrich trimethylation of Lys-27 on histone H3 at the *Tgf-β1* regulatory region and thereby maintains epigenetic silencing of *Tgf-β1* specifically within the second heart field-derived mesenchyme. Wild-type HDAC3 or catalytically inactive HDAC3 expression rescues aberrant endothelial-to-mesenchymal transition and epigenetic silencing of *Tgf-β1* in HDAC3-null outflow tracts and semilunar valves. These findings reveal that epigenetic dysregulation within the second heart field is a predisposing factor for congenital heart disease.

Congenital heart disease is the most common of all birth defects, the leading cause of infant mortality (1). Cardiac morphogenesis in the mouse begins at around embryonic day 7.0 (E7.0),[2] when a subset of cells derived from the antero-lateral mesoderm forms the cardiac crescent (2). This crescent contains the first and second heart field cardiac progenitor cells (3). The first heart field progenitor cells are the principal contributor to the primary heart tube, the left ventricle, atrioventricular canal, and atria (4). The second heart field progenitor cells extensively contribute to the outflow tract, semilunar valves, atria, right ventricle, primary atrial septum, and ventricular septum (5–9). Indeed, ablation or genetic manipulation of second heart field progenitor cells and their derivatives leads to outflow tract malrotation, overriding aorta, double outlet right ventricle, aberrant semilunar valve development, and ventricular septal defects (10–12). In humans, about two-thirds of congenital cardiac defects involve the outflow tract, semilunar valves, or ventricular septum (13).

Patterning of the second heart field requires several signaling pathways and their interaction with transcriptional regulators (14). Transforming growth factor-β (TGF-β) family members are among the pioneer signaling molecules that induce endothelial-to-mesenchymal transition (EndMT) to form semilunar valve cushions in the developing outflow tract (15–17). Subsequent elongation, expansion, and extracellular matrix remodeling transform these cushions into the mature semilunar valves (18–20). During these valvular remodeling processes, regulation of TGF-β bioavailability appears to be crucial. For instance, patients with semilunar valve pathologies, such as semilunar valve stenosis, regurgitation, and aberrant deposition of myofibroblasts and extracellular matrix, display elevated TGF-β levels (21–23). Indeed, exogenous TGF-β transforms cultured valvular interstitial cells into myofibroblasts and promotes excessive secretion of extracellular matrix (24–26). Elevated TGF-β level is also implicated in the pathogenesis of connective tissue disorders, such as Marfan syndrome, Ehlers-Danlos syndrome, and Loeys-Dietz syndrome (27–29). Interestingly, patients with these syndromes frequently display con-

* This work was supported by NHLBI, National Institutes of Health, Grant R01 HL118100 (to C. M. T.). The authors declare that they have no conflicts of interest with the contents of this article.
[1] To whom correspondence should be addressed: The Albert Sherman Center, AS7-1047, 368 Plantation St., Worcester, MA 01605. Tel.: 508-856-6947; Fax: 508-856-6933; E-mail: chinmay.trivedi@umassmed.edu.

[2] The abbreviations used are: E, embryonic day n; P0, postnatal day 0; HDAC, histone deacetylase; EndMT, endothelial-to-mesenchymal transition; IPA, Ingenuity Pathway Analysis; qPCR, quantitative PCR; H3K27, histone H3 Lys-27; H3K27me3, H3K27 trimethylation; H3K27ac, H3K27 acetylation.

genital cardiovascular anomalies, such as aortic dilatation, outflow tract defects, bicuspid aortic valve, semilunar valve stenosis, and ventricular septal defects (30–32). How the second heart field progenitor cells interpret elevated TGF-β at the chromatin level in these connective tissue disorders remains to be elucidated.

Extracellular matrix tightly regulates the bioavailability of active TGF-β (33). For instance, extracellular matrix proteoglycans, such as decorin (DCN), biglycan (BGN), and fibromodulin (FMOD), sequester TGF-β to limit its activity (34). Mice lacking DCN, BGN, or FMOD display elevated TGF-β activity and phenotypes observed in Marfan syndrome or Ehlers-Danlos syndrome (35–37). Indeed, proteoglycan deficiencies have been demonstrated in patients with these syndromes (38). Proteoglycans expressed in the developing outflow tract and semilunar valves also play a key role in the assembly of collagen fibers in the extracellular matrix (37, 39). Patients with collagen deficiency, such as COL3A1 mutations in Ehlers-Danlos syndrome, show elevated TGF-β levels (29). How extracellular matrix homeostasis is regulated remains an area of intense research.

The active form of TGF-β binds to TGFBR2 and TGFBR1, which in turn phosphorylate SMAD2/3 (R-SMADs) to promote assembly of heteromeric complex with SMAD4. Activated SMAD complex accumulates in the nucleus, where it recruits transcription co-factors and chromatin modifiers to regulate the expression of target genes (33). Several factors, in addition to TGF-β, play critical roles to trigger activation and amplification of the intracellular TGF-β signaling pathway at multiple levels (33). For instance, the transcription factor SNAI1 interacts with SMAD3/4 to repress endothelial gene expression and thereby augments TGF-β-mediated mesenchymal transition (40). EndMT, a specialized form of EMT, is the complex biological process in which endothelial cells trans-differentiate into mesenchymal cell types, including smooth muscle-like and fibroblast-like cells. EndMT has been implicated in several pathological processes, including fibrotic disorders and cardiac valvular diseases. A complex orchestration of several signaling pathways, including TGF-β signaling, initiates and promotes EndMT. However, the molecular and epigenetic mechanisms regulating termination of EndMT remain elusive.

Histone deacetylases (HDACs) are chromatin-modifying enzymes that regulate the epigenome (41). The mammalian HDACs are classified into five subfamilies based on their phylogenetic analysis and sequence homology. Class I HDACs (HDAC1, HDAC2, HDAC3, and HDAC8) play critical roles at various stages of development (42). For instance, global loss of HDAC1 or HDAC3 results in early embryonic lethality around E9.5 (42). Similarly, mice lacking HDAC2 or HDAC8 display lethality at birth (43–45). Our group and others, using gene inactivation studies in mice, have demonstrated vital functions for class I HDACs in cardiomyocyte proliferation, differentiation, and hypertrophy (43, 46–49). However, functions of HDACs in second heart field development remain undefined.

HDACs lack intrinsic DNA-binding domains but are recruited to the chromatin via their interaction with transcription factors, co-factors, and large multiprotein transcriptional complexes (41). For instance, HDAC3 is an integral part of NCOR (nuclear receptor corepressor) or its homologue SMRT (silencing mediator of retinoic and thyroid receptors). Interaction of HDAC3 with the deacetylase-activating domain of NCOR/SMRT is required for its enzyme activity. Interestingly, recent evidence suggests that enzymatic activity of HDAC3 is dispensable, but its interaction with NCOR/SMRT is essential for transcriptional repression. However, molecular mechanisms that mediate the deacetylase-independent function of HDAC3 remain to be defined. A recent study shows that HDAC4 controls histone methylation in response to elevated cardiac overload, suggesting that HDACs may recruit histone methyltransferases to the chromatin.

In this study, we demonstrate a deacetylase-independent role for HDAC3 as an epigenetic silencer of *Tgf-β1* within the second heart field with direct implications for human TGF-β pathway-associated cardiovascular anomalies. As a part of the NCOR complex, HDAC3 recruits EZH2 (enhancer of zeste homologue 2), the major histone methyltransferase of PRC2 (polycomb repressor complex 2), to mediate epigenetic silencing of *Tgf-β1* specifically within the second heart field-derived mesenchymal cells and thereby promotes termination of EndMT. Genetic deletion of *Hdac3* in the murine second heart field results in increased TGF-β bioavailability within mesenchymal cells, perpetual activation of mesenchymal cells, aberrant EndMT, and altered extracellular matrix homeostasis, observed in patients with semilunar valve pathologies. Together, these results uncover that epigenetic silencing mediated by HDAC3 in a deacetylase-independent manner orchestrates second heart field development, which may be a molecular target in human cardiovascular anomalies.

Experimental Procedures

Mice—Transgenic *Mef2C*-AHF-Cre, *Cdh5*-Cre, *Hdac3^{flox}*, and knock-in *Isl1*-Cre mice were described previously (7, 50–52). *Tagln*-Cre (Sm22α-Cre), *Myh6*-Cre (αMhc-Cre), and *R26R-LacZ* mice were obtained from the Jackson Laboratories. The University of Massachusetts Medical School Institutional Animal Care and Use Committee approved all animal protocols.

Histology—Tissue samples were fixed in 2% paraformaldehyde at 4 °C overnight, ethanol-dehydrated, embedded in paraffin, and sectioned at 6–8-μm thickness using a microtome.

Antibodies and Reagents—The following antibodies were used in this study: HDAC3 (Abcam and Santa Cruz Biotechnology), phospho-HDAC3 (Ser-424) (Cell Signaling), TGF-β pan-specific polyclonal antibody (R&D Systems), SMAD2/3 (Santa Cruz Biotechnology), phospho-SMAD2/3 (Ser-423/425) (Santa Cruz Biotechnology), vimentin (Santa Cruz Biotechnology), PECAM1 (BD Pharmingen), troponin T (Developmental Studies Hybridoma Bank, Iowa City, IA), MF-20 (Developmental Studies Hybridoma Bank, Iowa City, IA), cleaved caspase-3 (Cell Signaling), RNA polymerase II (Abcam), EZH2 (Abcam), NCOR1 (Abcam), H3K27ac (Abcam), H3K27me3 (Abcam), EED (Abcam), SUZ12 (Abcam), CREBBP (Abcam), IgG (R&D Systems), GAPDH (R&D Systems), FLAG (Sigma), α-tubulin (Sigma), IRDye-conjugated secondary antibodies (LI-COR), Alexa Fluor® 546-conjugated secondary antibody (Life Technologies), and biotinylated universal pan-specific antibody

(horse anti-mouse/rabbit/goat IgG) (Vector Laboratories). Recombinant TGF-β was purchased from R&D Systems. Alcian blue, alkaline alcohol, orcein, alcoholic hematoxylin, ferric chloride, Lugol's iodine, woodstain scarlet acid fuchsin, phosphotungstic acid, saffron, Bouin's fixative, Weigert's iron hematoxylin A, Weigert's iron hematoxylin B, phosphomolybdic acid-phosphotungstic acid, aniline blue, and Van Gieson's solution were purchased from Electron Microscopy Sciences. Harris modified hematoxylin, eosin Y, ethanol, xylenes, glacial acetic acid, paraformaldehyde, paraffin, potassium ferricyanide, potassium ferrocyanide, and deoxycholic acid were purchased from Fisher. Polyethylenimine, linear, was purchased from Polysciences. X-gal was purchased from 5 Prime. Vectashield mounting medium, the Vectastain Elite ABC kit, and the DAB Peroxidase Substrate kit were purchased from Vector Laboratories. The RNeasy minikit and GST bead slurry were purchased from Qiagen. Power SYBR Green PCR Master Mix, Superscript first strand synthesis kit, TOPO-TA cloning kit, DMEM high glucose with sodium pyruvate, penicillin/streptomycin, and horse serum were purchased from Invitrogen. The CellsDirect^{TM} one-step quantitative RT-PCR kit, insulin-transferrin-selenium, Epoxy M-450 Dynabeads, and TRIzol were purchased from Life Technologies, Inc. Rat tail collagen type I was purchased from BD Biosciences. iScript reverse transcription supermix was purchased from Bio-Rad. The sandwich ELISA assay kit for TGF-β1 was purchased from R&D Systems. The sandwich ELISA assay kit for phospho-SMAD2/3 was purchased from Cell Signaling. The QuikChange II XL site-directed mutagenesis kit was purchased from Stratagene. Passive lysis buffer and the Dual-Luciferase reporter assay kit were purchased from Promega. Fetal bovine serum, donkey serum, gelatin, and magnetic anti-FLAG beads were purchased from Sigma. Agarose-IgG and IgA bead slurry were purchased from Santa Cruz Biotechnology and Life Technologies. The EZ-ChIP assay kit and HDAC assay kit were purchased from Millipore. The TaKaRa DNA ligation kit was purchased from Clontech.

Hematoxylin and Eosin Staining—Hematoxylin and eosin staining was performed by deparaffinizing sections in xylenes, rehydrating through an ethanol gradient, 30-s or 2-min stain with 30% or 100% Harris modified hematoxylin, and a 30-s counterstain with eosin Y. Slides were rinsed and dehydrated with ethanol, cleared with xylenes, and mounted with Vectashield mounting medium.

Movat's Pentachrome Staining—Movat's pentachrome staining was conducted by deparaffinizing and rehydrating slides, followed by a 20-min stain in Alcian blue, a 1-h differentiation in alkaline alcohol, a 20-min stain in Orcein-Verhoeff solution (Orcein, alcoholic hematoxylin, ferric chloride, and Lugol's iodine), a 2-min stain with woodstain scarlet acid fuchsin, a rinse in acetic acid, and a 10-min differentiation in 5% phosphotungstic acid, followed by a 15-min stain in saffron. Sections were dehydrated in ethanol, cleared in xylenes, and mounted with Vectashield mounting medium.

Masson's Trichrome Staining—Masson's trichrome staining was performed by deparaffinizing and rehydrating sections through an ethanol gradient followed by a 1-h mordant in Bouin's fixative at 56 °C. Samples were then washed and stained for 5 min in a solution of Weigert's iron hematoxylin A and Weigert's iron hematoxylin B. Following washing, samples were differentiated in phosphomolybdic acid-phosphotungstic acid for 15 min, stained in aniline blue solution for 20 min, and differentiated in 1% acetic acid for 3 min. Samples were then dehydrated in ethanol, cleared in xylenes, and mounted with Vectashield mounting medium.

Modified Verhoeff Elastic-Van Gieson Stain—Modified Verhoeff Elastic-Van Gieson stain was conducted by deparaffinizing and rehydrating sections, staining for 7 min in Verhoeff working solution (1.8% alcoholic hematoxylin, 0.8% ferric chloride, 20% Lugol's iodine), washing in running water, differentiating for 1 min in 0.4% ferric chloride, and counterstaining for 3 min in Van Gieson's solution. Samples were then ethanol-dehydrated, cleared with xylenes, and mounted with Vectashield mounting medium.

LacZ Staining—Tissue samples were dissected in PBS and then fixed in 2% paraformaldehyde for 30 min at 4 °C. After washing in PBS at room temperature, samples were stained overnight in LacZ staining solution (5 mM potassium ferricyanide, 5 mM potassium ferrocyanide, 2 mM $MgCl_2$, 0.01% deoxycholic acid, 0.04% Nonidet P-40, 0.1% X-gal, in 1× PBS) at 37 °C in the dark. Samples were then washed in PBS and fixed overnight in 4% paraformaldehyde.

Plasmids and Site-directed Mutagenesis—FLAG-HDAC3 pcDNA3.1(−) and the FLAG-HDAC3 lentiviral vector were described previously (48). GFP lentiviral vector and lentiviral packaging plasmids were obtained from Addgene: pLOVE-GFP (Addgene plasmid 15949), pCMV-dR8.2 (Addgene plasmid 8455), and pCMV-VSVG (Addgene plasmid 8454). Lentiviral plasmids expressing HDAC3 shRNA, EZH2 shRNA, NCOR1 shRNA, and scrambled shRNA control were obtained from the University of Massachusetts shRNA Core Facility. FLAG-HDAC3^{H134A,H135A} was generated by site-directed mutagenesis as per the manufacturer's protocol, using FLAG-HDAC3 pcDNA3.1(−) as a template, and subcloned to CSCGW2. To generate the TGF-β1 luciferase construct, a 1309-bp promoter-proximal region immediately upstream of the translational start site of TGF-β1 was PCR-amplified from mouse genomic DNA, gel-purified, and cloned into pCR2.1 TOPO (Life Technologies), following the manufacturer's protocol. The promoter was subcloned from pCR2.1 TOPO to pGL3-basic (Promega). A 42-bp region containing an HDAC3 binding site, identified using published chromatin immunoprecipitation (ChIP)-sequencing data and confirmed by ChIP-qPCR from murine valve tissue, was deleted from the terminal 3′-end of the TGF-β1 promoter-proximal region (−42 to −1 relative to ATG) by PCR amplification using the TGF-β1 luciferase vector as a template. The 1267-bp TGF-β1 deletion promoter was gel-purified, cloned into pCR2.1 TOPO, and subcloned into pGL3-basic. All generated plasmids were verified by restriction analysis and sequencing.

Immunohistochemistry—For immunohistochemistry, sections were deparaffinized in xylenes and pretreated using heat antigen retrieval in sodium citrate buffer (10 mM sodium citrate, 0.05% Tween 20, pH 6). Immunohistochemistry was conducted using the Vectastain Elite ABC kit and DAB Peroxidase Substrate kit according to the manufacturers' guidelines. Sec-

tions were incubated with cleaved caspase-3 antibody (1:100) for 1 h at room temperature or HDAC3 antibody (1:250) or phospho-SMAD2/3 antibody (1:50) overnight at 4 °C. Biotinylated universal pan-specific antibody (horse anti-mouse/rabbit/goat IgG) was used for phospho-SMAD2/3 immunostaining in place of the Vectastain Elite ABC kit secondary antibody according to the manufacturer's guidelines. For counterstaining, slides were rinsed and then incubated with 30% hematoxylin for 30 s after 3,3′-diaminobenzidine developing. All slides were ethanol-dehydrated, cleared with xylenes, and mounted with Vectashield mounting medium. For immunofluorescent staining, sections were deparaffinized and rehydrated through xylenes and an ethanol gradient. Slides were rinsed in PBS, and antigen retrieval was performed in sodium citrate buffer (10 mM sodium citrate, 0.05% Tween 20, pH 6.0) for 10 min at 95 °C. After rinsing, sections were blocked in 10% donkey serum, 0.3% Triton X-100 in PBS for 1 h at room temperature. Sections were then washed in PBS and incubated with smooth muscle actin antibody (1:100) in 10% donkey serum and PBS for 1 h at room temperature or with MF-20 (1:50) or troponin (1:25) antibodies in 10% donkey serum in PBS overnight at 4 °C. Finally, slides were washed in PBS, incubated in secondary antibody (donkey anti-mouse 546, 1:500, with Hoechst, 1:1000, in 10% donkey serum, PBS) for 1 h at room temperature, rinsed in PBS, and mounted with Vectashield mounting medium.

Biometric Analysis—Aortic diameter was measured from ×2 images of dissected hearts at three levels (tubular aortic trunk, proximal aortic arch, and intermediate aortic arch) using NIS-Elements analysis software (Nikon). Ventricular wall thickness and valve area measurements were made from ×2 and ×10 images, respectively, of position-matched hematoxylin and eosin-stained sections using NIS-Elements analysis software (Nikon). Nuclei numbers per section in the valves were counted manually in ×10 hematoxylin and eosin-stained sections using ImageJ counting tools. Differences between groups were compared using Student's *t* tests.

Real-time Quantitative PCR—Total RNA was extracted and reverse transcribed using iScript reverse transcription supermix (Bio-Rad) or the CellAmp whole transcriptome amplification kit (Takara) according to the manufacturer's guidelines. Transcript expression was measured by quantitative RT-PCR using SYBR Green PCR Master Mix. Signals were normalized to corresponding GAPDH controls and represented as relative expression ratios of experimental samples relative to $Hdac3^{F/F}$ controls. Primer sequences are available upon request.

Apoptosis Assay—Sections of aortic and pulmonic valves from five $Hdac3^{Isl1KO}$ and five control E13.5 hearts were immunostained with cleaved caspase-3 antibody and counterstained with hematoxylin. Images of the aortic and pulmonic valves were taken at ×20 magnification. The total number of nuclei and the number of cleaved caspase-3 positive nuclei within the valve cusp were manually counted for each sample. The aortic and pulmonic valves were compared separately. The number of cleaved caspase-3-positive nuclei per 1000 nuclei served as an apoptosis index.

Microarray Analysis—Heart tissue was dissected from E9.5 mouse embryos and snap-frozen in liquid nitrogen. RNA was extracted from pools of $Hdac3^{Isl1KO}$ or $Hdac3^{F/F}$ control hearts using an RNeasy minikit. Microarray analysis was performed in triplicate from pooled samples by the University of Massachusetts Genomics Core Facility using Affymetrix Mouse Gene 2.0 ST arrays (Affymetrix). Raw microarray data were annotated using the Bioconductor and Oligo packages in R (53–55). Significance of expression differences between $Hdac3^{Isl1KO}$ and $Hdac3^{F/F}$ samples was determined using Student's *t* test. Heat maps of microarray data were generated using the pheatmap package in R (56). Relative expression of each transcript is reported as log-transformed expression value for each sample, normalized to the median expression value of the transcript across all six samples. MIAME-compliant full microarray data sets can be accessed at the Gene Expression Omnibus (GEO, GSE73666).

Ingenuity Pathway Analysis—Microarray data from E9.5 $Hdac3^{Isl1KO}$ and control hearts were analyzed using Ingenuity Pathway Analysis (IPA). The IPA Diseases and Functions utility was employed to investigate phenotypes associated with the molecular changes. Hierarchical heat maps were generated using both the Diseases and Biological Functions categories and Tox Functions categories of the Diseases and Functions utility. Plots of phenotypically relevant categories were constructed based on subcategory *p* values. The Upstream Regulators utility was employed to determine potential regulators of differentially expressed genes. Significant regulators were sorted by significance and by number of associated genes. Differentially expressed genes associated with the upstream regulator TGF-β1 were exported, and a clustered heat map was generated using R software.

Lentiviral Infection—Lentiviral medium was generated by transfecting 100-mm plates of subconfluent 293T cells with 5 μg of lentiviral cDNA, 5 μg of pCMV-dR8.2, and 2.5 μg of pCMV-VSVG, in 10 ml of 2% FBS medium. The medium was changed to a fresh 10 ml of 2% FBS medium 24 h after transfection. Viral medium was collected 24 h later and filtered through a 40-μm cell strainer. Isolated mouse embryonic heart tissue was infected with filtered viral medium supplemented with 10 μg/ml Polybrene reagent. GFP viral medium was used to maintain a constant viral medium volume. Infected cells were harvested for analysis 24 or 48 h after infection.

Cell Culture, Transient Transfection, and Luciferase Assay—HEK293T cells and murine endothelial cells were maintained in DMEM with 10% FBS, 100 mg/ml penicillin, and 100 mM/ml streptomycin in a 37 °C incubator with 5% CO_2. HEK293T cells were transfected in subconfluent 100-mm plates with 2.5 μg of DNA and 5 μl of polyethylenimine, linear, in 10 ml of 10% FBS medium. Luciferase assays were conducted by transfecting subconfluent murine endothelial cells in 6-well plates with 1 μg of DNA and 2 μl of polyethylenimine, linear, in 2 ml of 10% FBS medium. The DNA amount was maintained constant using pcDNA3.1(−) or pLJM1-EGFP DNA. Cells were lysed with passive lysis buffer 16 h after transfection, and lysates were analyzed using the Dual-Luciferase reporter assay kit according to the manufacturer's guidelines. Luciferase activity was measured using a Berthold microplate reader according to the manufacturer's guidelines.

Immunoprecipitation—Tissue samples were homogenized in immunoprecipitation buffer (50 mM Tris-HCl (pH 8.0), 150 mM NaCl, 0.5% Nonidet P-40, 1 mM EDTA, and 1 mM DTT) containing 1 mM PMSF, phosphate inhibitors (Sigma), and protease inhibitor mixture (Sigma). The homogenized samples were sonicated using a Branson 250 Digital Sonifier with 1-s on and 1-s off pulses at 40% power amplitude for 15 s. Precleared lysates with beads were incubated with primary antibodies for 16 h at 4 °C. After incubation for 1 h at 4 °C with beads, immune complexes were collected, washed four times with immunoprecipitation buffer, and applied to 4–12% SDS-polyacrylamide gels for Western blot analysis.

Western Blotting—Tissue lysates were prepared in lysis buffer (20 mM Tris-HCl (pH 7.5), 15 mM NaCl, 1 mM Na_2EDTA, 1 mM EGTA, 1% Triton X-100, 1 μg/ml leupeptin, 2.5 mM sodium pyrophosphate, 1 mM Na_3VO_4, and 1 mM β-glycerophosphate; 1 mM phenylmethylsulfonyl fluoride was added before use). Protein samples were resolved on 4–12% SDS-PAGE acrylamide gel before transferring to PVDF membranes. We used primary antibodies to HDAC3 (1:1000) and FLAG (1:1000). Primary antibodies were visualized by chemiluminescence using HRP-conjugated secondary antibodies or by infrared with IRDye®-conjugated secondary antibodies. Blots were probed with α-tubulin (1:1000) or GAPDH (1:1000) for loading control.

ELISA—Sandwich ELISAs were performed according to the manufacturer's protocol. Briefly, for the phospho-SMAD2/3 or phospho-HDAC3 ELISA, samples were prepared using 100 μl of 1× cell lysis buffer (20 mM Tris, pH 7.5, 150 mM NaCl, 1 mM EDTA, 1 mM EGTA, 1% Triton X-100, 2.5 mM sodium pyrophosphate, 1 mM β-glycerophosphate, 1 mM Na_3VO_4, 1 μg/ml leupeptin). 100 μl of sample diluent was added per 100 μl of sample (1:1 ratio). Samples were incubated overnight at 4 °C. After four washes with 1× wash buffer, samples were incubated with detection antibody for 1 h at 37 °C. Samples were visualized using the HRP detection method at 450 nm. For the phospho-HDAC3 ELISA, a microtiter plate was coated with HDAC3 antibody (5 μg/ml) in carbonate/bicarbonate buffer (pH 9.6). The sandwich ELISA for TGF-β1 was performed according to the manufacturer's protocol. Briefly, samples were prepared using assay diluent buffer RD1-21. Samples were incubated for 2 h at room temperature. After four washes with 1× wash buffer, samples were incubated with 100 μl of TGF-β1 conjugate for 2 h at room temperature. After four washes with 1× wash buffer, samples were incubated with 100 μl of substrate solution (protected from light) for 30 min at room temperature. After the addition of 100 μl of stop solution, reactions were visualized at 450 and 540 nm. Readings at 540 nm were subtracted from readings at 450 nm to correct for optical imperfections in the plate.

Outflow Tract Explant Assay—The outflow tract explant cultures were performed as described previously (57, 58). Briefly, a solution of rat tail collagen type I (1.5 mg/ml) containing NaOH to a final concentration of 15 mmol/liter was dispensed into 24-well microculture dishes. Subsequently, gels were placed in a 37 °C tissue culture incubator at 5% CO_2 and allowed to polymerize. After 30 min, collagen gels were washed several times with DMEM containing 10% fetal bovine serum, 0.1% insulin-transferrin-selenium, 100 mg/ml penicillin, and 100 mM/ml streptomycin. Outflow tracts were carefully dissected from control and *Hdac3*^{Isl1KO} E9.5, E10.5, or E14.5 embryonic hearts. The outflow tracts were placed endocardium face down onto collagen gels and allowed to adhere for 8 h at 37 °C in 5% CO_2. Eight hours after attachment, medium was added, and explants were cultured for up to 24, 48, or 72 h. Radial migration was measured from ×4 images of outflow tract explants at 45° intervals using NIS-Elements analysis software (Nikon). Explants were treated with TGF-β antibody (1 μg/ml) for 24 or 48 h or with recombinant TGF-β (10 ng/ml) for 24 or 48 h. Explants were also detached, trypsinized, and incubated with anti-vimentin (mesenchymal marker) antibody-conjugated or PECAM-1 (endothelial marker)-conjugated epoxy M-450 Dynabeads as per the manufacturer's guidelines to isolate cells.

ChIP Analysis—ChIP experiments were performed as described previously (48). Briefly, isolated cardiac tissue or explants from E9.5 mouse embryos were cross-linked for 15 min in cross-linking solution (1% formaldehyde, 1.5 mM ethylene glycol-bis succinimidylsuccinate, 20 mM sodium butyrate, 10% FBS) and then quenched with 125 mM glycine solution for 5 min, followed by two washes with 1× PBS. Chromatin fragmentation was carried out by sonication in ChIP SDS lysis buffer (50 mM Tris-HCl, pH 8.0, 10 mM EDTA, 1% SDS, 1× protease inhibitors), using the Branson Sonifier 250 (40% power amplitude, 110 s). Proteins were immunoprecipitated in ChIP dilution buffer (0.01% SDS, 1.1% Triton X-100, 1.2 mM EDTA, 16.7 mM Tris-HCl, pH 8.0, 167 mM NaCl, 20 mM sodium butyrate, 1× protease inhibitor) using IgG, HDAC3, NCOR1, EZH2, H3K27me3, H3K27ac, polymerase II, EED, SUZ12, or CREBBP antibody. Specificity of HDAC3, NCOR1, EZH2, H3K27me3, H3K27ac, polymerase II, EED, SUZ12, or CREBBP antibody at the relevant loci was determined using IgG control antibody. Specificity of HDAC3 antibody at the relevant loci was also determined using HDAC3-null hearts compared with wild-type control. Immunoprecipitated antibody-chromatin complexes were washed twice with low salt wash buffer (20 mM Tris-HCl, pH 8.0, 150 mM NaCl, 2 mM EDTA, 0.1% SDS, and 1% Triton X-100) followed by two washes with lithium chloride wash buffer (10 mM Tris-HCl, pH 8.0, 250 mM LiCl, 1 mM EDTA, 1% deoxycholate, and 1% Nonidet P-40) and TE buffer (10 mM Tris-HCl, pH 8.0, and 1 mM EDTA). After removing wash buffer, cross-linking was reversed at 65 °C overnight in Proteinase K buffer (20 mM Tris-HCl, pH 7.5, 5 mM EDTA, 50 mM NaCl, 1% SDS, 20 mM sodium butyrate, 50 μg/ml Proteinase K). The following day, DNA was purified using phenol/chloroform/isoamyl alcohol. Purified precipitated DNA was analyzed by quantitative RT-PCR as described previously. Enrichment
of target sequences was determined by quantitative RT-PCR using primers designed against HDAC3 consensus binding sites within the proximal 10 kb upstream of the transcription start site of genes of interest: *Tgf-β1*, *Kpnb1*, *Sumo1*, and *Smad4*. Primer sequences are available upon request.

HDAC Activity Assay—HDAC activity was measured by using an HDAC activity assay kit for fluorometric detection as per the manufacturer's protocol. Briefly, 293T cells were transfected with or without plasmid containing either HDAC3-

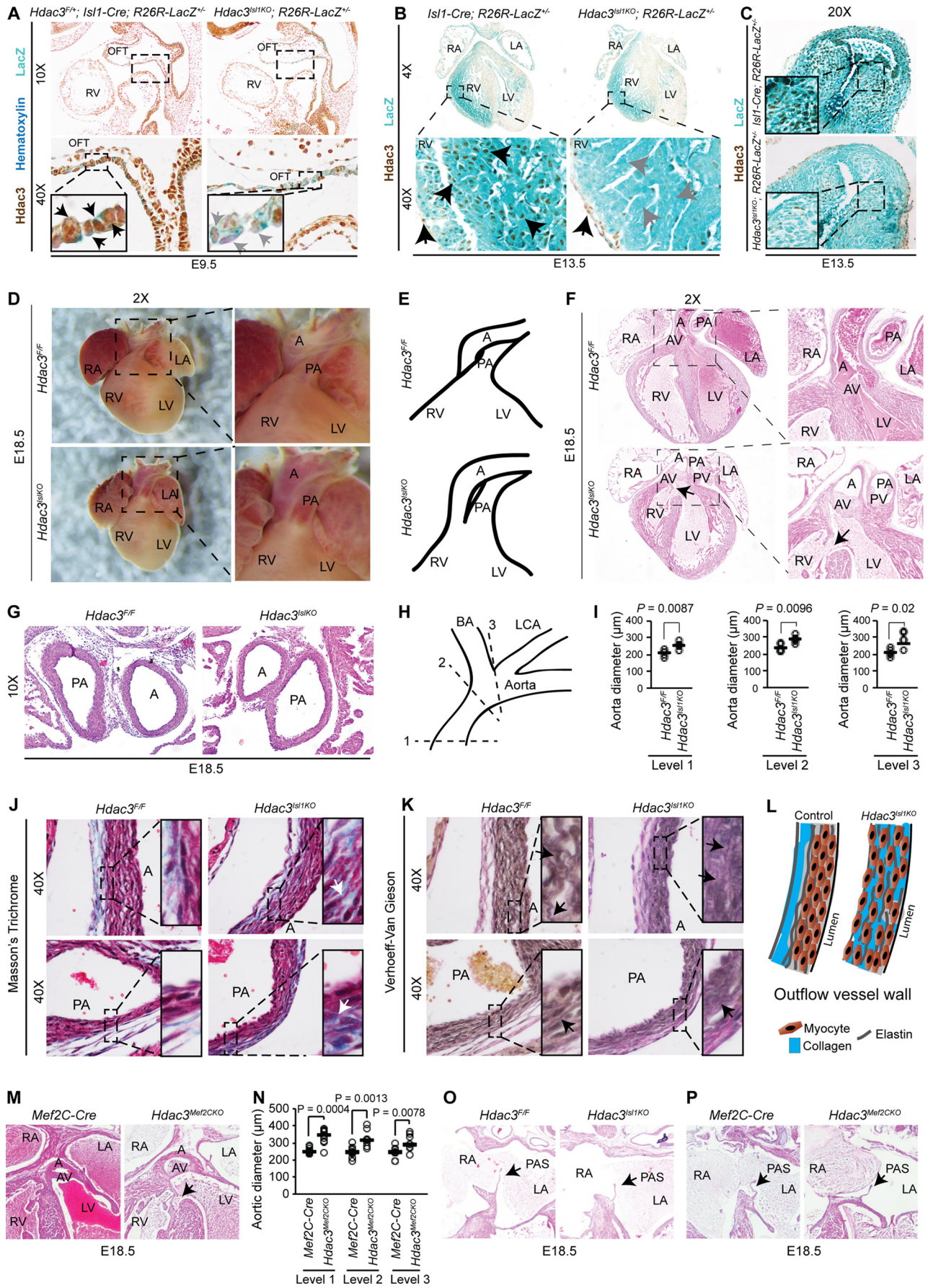
A
Hdac3F/+; Isl1-Cre; R26R-LacZ+/-
Hdac3Isl1KO; R26R-LacZ+/-
LacZ
Hematoxylin
Hdac3
10X
40X
OFT
RV
E9.5
B
Isl1-Cre; R26R-LacZ+/-
Hdac3Isl1KO; R26R-LacZ+/-
4X
40X
RA
LA
RV
LV
E13.5
C
20X
Hdac3Isl1KO; R26R-LacZ+/-; Isl1-Cre; R26R-LacZ+/-
E13.5
D
2X
Hdac3F/F
Hdac3IslKO
E18.5
A
PA
RA
LA
RV
LV
E
F
2X
AV
PV
PA
E18.5
G
Hdac3F/F
Hdac3IslKO
10X
PA
A
E18.5
H
BA
3
LCA
2
Aorta
1
I
P = 0.0087
P = 0.0096
P = 0.02
Aorta diameter (μm)
400
300
200
100
0
Hdac3F/F
Hdac3Isl1KO
Level 1
Level 2
Level 3
J
Hdac3F/F
Hdac3Isl1KO
Masson's Trichrome
40X
K
Verhoeff-Van Gieson
L
Control
Hdac3Isl1KO
Lumen
Outflow vessel wall
Myocyte
Collagen
Elastin
M
Mef2C-Cre
Hdac3Mef2CKO
AV
LV
E18.5
N
P = 0.0013
P = 0.0004
P = 0.0078
Aortic diameter (μm)
500
400
300
200
100
0
Mef2C-Cre
Hdac3Mef2CKO
Level 1
Level 2
Level 3
O
Hdac3F/F
Hdac3Isl1KO
PAS
E18.5
P
Mef2C-Cre
Hdac3Mef2CKO
E18.5

TABLE 1
Genotyping of *Isl1-Cre; Hdac3$^{F/+}$* × *Hdac3$^{F/+}$*

	Observed (Expected)	
	E18.5	P0
Hdac3$^{+/+}$	9 (9)	18 (11)
Hdac3$^{F/+}$	17 (18)	22 (22)
Hdac3$^{F/F}$	11 (9)	12 (11)
Isl1-Cre; Hdac3$^{+/+}$	13 (9)	17 (11)
Isl1-Cre; Hdac3$^{F/+}$	15 (18)	19 (22)
Isl1-Cre; *Hdac3$^{F/F}$*	7 (9)	0 (11)
Total	72	88
χ^2	NS[a]	$p < 0.01$

[a] Not significant.

FLAG or HDAC3^{H134A,H135A}-FLAG. Using anti-FLAG antibody, total lysate was immunoprecipitated and then incubated with HDAC assay substrate for 60 min at 37 °C. After the addition of diluted activator reagent, samples were incubated at room temperature for 10 min and analyzed by a fluorescent microplate reader at excitation of 360 nm and emission of 450 nm.

Statistical Analysis—Statistical significance between groups was determined using two-tailed Student's *t* test or χ^2 test. A *p* value of <0.05 was considered significant.

Results

HDAC3 Is Required in the Second Heart Field for Cardiac Development—Germ line deletion of ubiquitously expressed HDAC3 results in embryonic lethality at E9.5 (59, 60). To determine the function of HDAC3 in the second heart field, we deleted HDAC3 in the second heart field progenitor cells using two Cre lines, *Isl1-Cre* (*Hdac3^{Isl1KO}*) (Fig. 1, *A–C*) and *Mef2C-Cre* (*Hdac3^{Mef2CKO}*) (7, 50). *Hdac3^{Isl1KO}* embryos were identified at E18.5 (Table 1). However, *Hdac3^{Isl1KO}* pups displayed complete lethality at birth (P0) ($p < 0.01$; Table 1). *Hdac3^{Isl1KO}* embryos were characterized by malrotation of outflow tract, overriding aorta, double outlet right ventricle, membranous ventricular septal defect, ascending aortic dilatation (21–35%, $p < 0.02$), and normal outflow tract septation at E18.5 (Table 2 and Fig. 1, *D–I*). *Hdac3^{Isl1KO}* embryos displayed aberrant distribution and expression of collagen in all layers of ascending aortic and pulmonary arterial walls (Fig. 1, *J–L*). In addition, elastin fibers appeared fragmented, probably explaining aortic dilatation in *Hdac3^{Isl1KO}* embryos (Fig. 1, *K* and *L*). *Isl1-Cre* is a knock-in allele; however, we did not observe genetic interaction between HDAC3 and ISL1 (Tables 1 and 2). *Hdac3^{Mef2CKO}* embryos revealed similar developmental cardiac defects, including double outlet right ventricle, ascending aortic dilatation (22–32%, $p < 0.002$), and perinatal lethality (Tables 2 and 3 and Fig. 1, *M* and *N*). Primary atrial septum and right ventricle, in part derived by the second heart field progenitor cells, appeared normal in both *Hdac3^{Isl1KO}* and *Hdac3^{Mef2CKO}* hearts (Fig. 1, *O* and *P*) (data not shown). Cardiomyocyte differentiation was unaffected in early *Hdac3^{Isl1KO}* embryos (data not shown).

HDAC3 Is Essential for Semilunar Valve Development—The second heart field progenitor cells are required for conotruncal cushion development, which contributes to the semilunar valves and outflow tract septum (5, 6, 8–10). *Hdac3^{Isl1KO}* embryos demonstrated dysmorphic, thickened (1.59–3-fold, $p < 0.02$), and hyperplastic (1.31–3.14-fold, $p < 0.02$) semilunar valves at E18.5 (Table 2 and Fig. 2, *A–N*). Interestingly, aortic valves were bicuspid in *Hdac3^{Isl1KO}* hearts (Table 2 and Fig. 2*E*). The outflow tract septum and atrioventricular valves appeared normal in these embryos at E18.5 (Figs. 1*G* and 2*O*). Similarly, *Hdac3^{Mef2CKO}* embryos revealed defects in semilunar valve development, but not in atrioventricular valve development, at E18.5 (Table 2 and Fig. 2, *P–T*).

The mature semilunar valves are composed of extracellular matrix, valvular interstitial cells, and endothelial cells. Remodeling of valvular interstitial cells and extracellular matrix, mainly collagens, proteoglycans, and elastin, is essential for maturation of the semilunar valves (61). *Hdac3^{Isl1KO}* hearts displayed loss of extracellular matrix trilaminar stratification and valvular interstitial cell compartmentalization in the semilunar valves at various stages of development (Fig. 3, *A–F*, *L*, and *M*). Specifically, loss of HDAC3 resulted in aberrant expression of collagen and proteoglycan in all layers, probably explaining enlarged and thickened semilunar valves (Fig. 3, *A–F*, *L*, and *M*). Elastin fibers appeared disorganized and fragmented in *Hdac3^{Isl1KO}* semilunar valves (Fig. 3, *A*, *B*, *E*, *F*, *L*, and *M*). Similarly, *Hdac3^{Mef2CKO}* embryos revealed aberrant expression of collagen and proteoglycan in all layers of the semilunar valves (Fig. 3, *G* and *H*). Remodeling of the semilunar valves is associated with an increase in apoptosis (18). *Hdac3^{Isl1KO}* semilunar valve interstitial cells displayed a 55–65% decrease in apoptosis compared with controls ($p < 0.02$) during valve remodeling (Fig. 3, *I–K*).

HDAC3 Regulates TGF-β Signaling Pathway—Transcriptional analysis of early embryonic *Hdac3^{Isl1KO}* hearts revealed significant expression changes indicative of the

FIGURE 1. **HDAC3 functions within the second heart field to regulate cardiac morphogenesis.** *A–C*, HDAC3 immunostaining of LacZ-stained *Hdac3^{Isl1KO}*; *R26R-LacZ$^{+/-}$* and control embryos shows that HDAC3 protein expression (*black arrows*) is lost (*gray arrows*) in the *Isl1*-Cre expression domain in E9.5 (*A*) and E13.5 (*B* and *C*) *Hdac3^{Isl1KO}* hearts, including in semilunar valves (*C*). *D*, dissected and fixed E18.5 hearts show malrotation of the outflow tract in *Hdac3^{Isl1KO}* hearts. *E*, tracings of outflow tract vessels demonstrate abnormal, parallel orientation of the aorta and pulmonary artery in *Hdac3^{Isl1KO}* hearts. *F*, hematoxylin- and eosin-stained sections demonstrate double outlet right ventricle, with membranous ventricular septal defect (*arrow*) and an overriding aorta in *Hdac3^{Isl1KO}* E18.5 hearts. *G*, hematoxylin- and eosin-stained cross-sections show malrotation but complete septation of the aorta and pulmonary artery in E18.5 *Hdac3^{Isl1KO}* hearts. *H* and *I*, schematic diagram of proximal aorta showing three levels: level 1 (tubular aortic trunk), level 2 (proximal aortic arch), and level 3 (intermediate aortic arch) (*H*). Shown is a comparison of aorta diameter in *Hdac3^{Isl1KO}* and control hearts, measured at three levels from dissected, fixed hearts (*I*). *J*, Masson's trichrome-stained sections of aorta and pulmonary artery demonstrate disorganized collagen (*blue*) in the vessel walls of *Hdac3^{Isl1KO}* E18.5 hearts. *K*, Verhoeff-Van Gieson-stained sections of aorta and pulmonary artery demonstrate disorganized collagen (*arrows*, *red*) and fragmented elastin (*arrows*, *black*) in the vessel walls of *Hdac3^{Isl1KO}* E18.5 hearts. *L*, schematic model of disorganized outflow vessel wall morphology. *M*, hematoxylin- and eosin-stained sections demonstrate double outlet right ventricle with aortic valve overriding a membranous ventricular septal defect (*arrow*) in *Hdac3^{Mef2CKO}* E18.5 hearts. *N*, quantification of aortic diameter shows dilation of E18.5 *Hdac3^{Mef2CKO}* aortas at three levels: level 1 (tubular aortic trunk), level 2 (proximal aortic arch), and level 3 (intermediate aortic arch). *O* and *P*, hematoxylin- and eosin-stained sections show normal primary atrial septum (*arrow*) in *Hdac3^{Isl1KO}* (*O*) and *Hdac3^{Mef2CKO}* E18.5 hearts (*P*). *RA*, right atrium; *LA*, left atrium; *A*, aorta; *AV*, aortic valve; *PA*, pulmonary artery; *PV*, pulmonic valve; *RV*, right ventricle; *LV*, left ventricle; *BA*, brachiocephalic artery; *LCA*, left common carotid artery; *PAS*, primary atrial septum.

TABLE 2
Phenotypes of mice, age E18.5–P0

Genotype	Incidence	Total	χ^2 test	p
Outflow tract malrotation				
Hdac3^{Isl1KO}	6	6	*Hdac3^{Isl1KO}* (6/6): *Hdac3$^{F/F}$* (0/6)	0.014
Hdac3^{Mef2CKO}	8	9	*Hdac3^{Mef2CKO}* (8/9): *Hdac3$^{F/F}$* (0/6)	0.0209
Hdac3^{TaglnKO}	3	3	*Hdac3^{TaglnKO}* (3/3): *Hdac3$^{F/F}$* (0/4)	0.045
Hdac3$^{F/+}$; Isl1-Cre	0	4	Hdac3$^{F/+}$; Isl1-Cre (0/4): Hdac3$^{F/F}$ (0/6)	1
Double outlet right ventricle				
Hdac3^{Isl1KO}	5	6	*Hdac3^{Isl1KO}* (5/6): *Hdac3$^{F/F}$* (0/6)	0.0253
Hdac3^{Mef2CKO}	3	3	*Hdac3^{Mef2CKO}* (3/3): *Hdac3$^{F/F}$* (0/6)	0.014
Hdac3^{TaglnKO}	3	3	*Hdac3^{TaglnKO}* (3/3): *Hdac3$^{F/F}$* (0/4)	0.045
Hdac3$^{F/+}$; Isl1-Cre	0	4	*Hdac3$^{F/+}$; Isl1-Cre* (0/4): *Hdac3$^{F/F}$* (0/6)	1
Ventricular septal defect				
Hdac3^{Isl1KO}	6	6	*Hdac3^{Isl1KO}* (6/6): *Hdac3$^{F/F}$* (0/6)	0.014
Hdac3^{Mef2CKO}	5	5	*Hdac3^{Mef2CKO}* (5/5): *Hdac3$^{F/F}$* (0/6)	0.014
Hdac3^{TaglnKO}	3	3	*Hdac3^{TaglnKO}* (3/3): *Hdac3$^{F/F}$* (0/4)	0.045
Hdac3$^{F/+}$; Isl1-Cre	0	4	*Hdac3$^{F/+}$; Isl1-Cre* (0/4): *Hdac3$^{F/F}$* (0/6)	1
Overriding aorta				
Hdac3^{Isl1KO}	5	6	*Hdac3^{Isl1KO}* (5/6): *Hdac3$^{F/F}$* (6/6)	0.0253
Hdac3^{Mef2CKO}	3	3	*Hdac3^{Mef2CKO}* (3/3): *Hdac3$^{F/F}$* (0/6)	0.014
Hdac3^{TaglnKO}	3	3	*Hdac3^{TaglnKO}* (3/3): *Hdac3$^{F/F}$* (0/4)	0.045
Hdac3$^{F/+}$; Isl1-Cre	0	4	*Hdac3$^{F/+}$; Isl1-Cre* (0/4): *Hdac3$^{F/F}$* (0/6)	1
Hyperplastic aortic valve				
Hdac3^{Isl1KO}	12	12	*Hdac3^{Isl1KO}* (12/12): *Hdac3$^{F/F}$* (0/12)	0.00053
Hdac3^{Mef2CKO}	9	9	*Hdac3^{Mef2CKO}* (9/9): *Hdac3$^{F/F}$* (0/12)	0.00053
Hdac3^{TaglnKO}	3	3	*Hdac3^{TaglnKO}* (3/3): *Hdac3$^{F/F}$* (0/4)	0.045
Hdac3$^{F/+}$; Isl1-Cre	0	8	*Hdac3$^{F/+}$; Isl1-Cre* (0/8): *Hdac3$^{F/F}$* (0/12)	1
Hyperplastic pulmonic valve				
Hdac3^{Isl1KO}	12	12	*Hdac3^{Isl1KO}* (12/12): *Hdac3$^{F/F}$* (0/12)	0.00053
Hdac3^{Mef2CKO}	9	9	*Hdac3^{Mef2CKO}* (9/9): *Hdac3$^{F/F}$* (0/12)	0.00053
Hdac3^{TaglnKO}	3	3	*Hdac3^{TaglnKO}* (3/3): *Hdac3$^{F/F}$* (0/4)	0.045
Hdac3$^{F/+}$; Isl1-Cre	0	8	*Hdac3$^{F/+}$; Isl1-Cre* (0/8): *Hdac3$^{F/F}$* (0/12)	1
Bicuspid aortic valve				
Hdac3^{Isl1KO}	4	4	*Hdac3^{Isl1KO}* (4/4): *Hdac3$^{F/F}$* (0/6)	0.014
Hdac3^{Mef2CKO}	3	3	*Hdac3^{Mef2CKO}* (3/3): *Hdac3$^{F/F}$* (0/6)	0.014
Hdac3$^{F/+}$; Isl1-Cre	0	4	*Hdac3$^{F/+}$; Isl1-Cre* (0/4): *Hdac3$^{F/F}$* (0/6)	1

TABLE 3
Genotyping of *Mef2c-Cre; Hdac3$^{F/+}$* × *Hdac3$^{F/+}$*

	Observed (Expected)	
	E18.5	P0
Hdac3$^{+/+}$	14 (8)	10 (12)
Hdac3$^{F/+}$	12 (16)	23 (24)
Hdac3$^{F/F}$	6 (8)	12 (12)
Mef2c-Cre; Hdac3$^{+/+}$	10 (8)	18 (12)
Mef2c -Cre; Hdac3$^{F/+}$	13 (16)	30 (24)
Mef2c-Cre; Hdac3$^{F/F}$	9 (8)	3 (12)
Total	64	96
χ^2	NS[a]	$p = 0.04$

[a] Not significant.

congenital heart defects observed in late stage *Hdac3^{Isl1KO}* embryos (Fig. 4, *A* and *B*). Upstream regulator analysis identified marked changes in TGF-β1 pathway genes (Fig. 4, *C–E*). Positive regulators of the TGF-β pathway, including *Sumo1*, *Nrp2*, *Smad4*, *Snai1*, *Tgf-β1*, and *Kpnb1* were 3–9-fold up-regulated ($p < 0.02$) in *Hdac3^{Isl1KO}* hearts (Fig. 4*F*). ChIP-qPCR analysis confirmed chromatin occupancy of HDAC3 (0.15–0.5%, $p < 0.002$) on identified sites in the conserved noncoding regions within 10 kb upstream of TGF-β pathway genes, including *Smad4*, *Sumo1*, *Tgf-β1*, and *Kpnb1* (Fig. 4, *G–J*). We also observed ~3.5-fold higher TGF-β levels in *Hdac3^{Isl1KO}* outflow tracts compared with control ($p < 0.015$; Fig. 4*K*). Loss of HDAC3 resulted in ~2.7-fold activation of SMAD2/3 phosphorylation ($p < 0.02$), suggesting enhanced TGF-β signaling (Fig. 4, *L* and *M*). These results suggest that HDAC3 represses TGF-β signaling pathway during early cardiogenesis.

TGF-β Mediates Aberrant EndMT and Extracellular Matrix Remodeling in Hdac3^{Isl1KO} Heart—TGF-β signaling and its downstream target genes, such as *Snai1*, are critical factors that induce EndMT in the developing outflow tract cushions (40). EndMT is characterized by loss of endothelial markers, such as TEK, and gain of mesenchymal markers, such as TAGLN (33). *Hdac3^{Isl1KO}* hearts exhibited robust down-regulation of *Tek* and up-regulation of *Snai1* and *Tagln* (Figs. 4*F* and 5*A*). *Hdac3^{Isl1KO}* outflow tract cushion explants showed ~3-fold induction of EndMT ($p < 0.005$; Fig. 5, *B* and *C*), and these changes were largely abolished by TGF-β-neutralizing antibody ($p < 0.009$; Fig. 5, *B–F*). Aberrant TGF-β signaling activates valvular interstitial cells, which in turn, express smooth muscle genes and produce extracellular matrix scaffold proteins to remodel valvular matrix (24). *Hdac3^{Isl1KO}* hearts revealed significant expression changes in smooth muscle and extracellular matrix genes (Fig. 5, *A* and *G–M*). Smooth muscle genes, including *Tagln*, *Myh11*, and *Cnn2*, were up-regulated in *Hdac3^{Isl1KO}* hearts and semilunar valves (Fig. 5, *A*, *G*, and *H*). Simultaneously, expression of proteoglycans, including *Dcn*, *Bgn*, *Fmod*, and *Vcan*, and collagens, including *Col2a1*, *Col11a2*, *Col9a2*, *Col1a2*, and *Col3a1*, were significantly altered in *Hdac3^{Isl1KO}* hearts and semilunar valves (Fig. 5, *A* and *I–M*). We next examined the requirement of TGF-β for aberrant expression of extracellular matrix genes in *Hdac3^{Isl1KO}* valvular interstitial cells. Loss of HDAC3 resulted in 6–10-fold expression changes in proteoglycans, collagen, and smooth muscle genes ($p < 0.006$), and these changes were largely abol-

ished by TGF-β-neutralizing antibody (Fig. 5, *H–M*). Taken together, these results suggest that aberrant EndMT and extracellular matrix remodeling in *Hdac3*^{Isl1KO} hearts are mediated by TGF-β signaling.

HDAC3 Functions within Mesenchymal or Smooth Muscle Cells to Regulate Semilunar Valve and Outflow Tract Development—The second heart field progenitor cells give rise to cardiomyocytes, endothelial cells, and mesenchymal cells or smooth muscle cells (62, 63). Genetic deletion of *Hdac3* using *Cdh5-Cre* (*Hdac3*^{Cdh5KO}), which is expressed in differentiated endothelial and endocardial cells at E8.0 (52), and *Myh6-Cre* (*Hdac3*^{Myh6KO}), which is expressed in differentiated car-

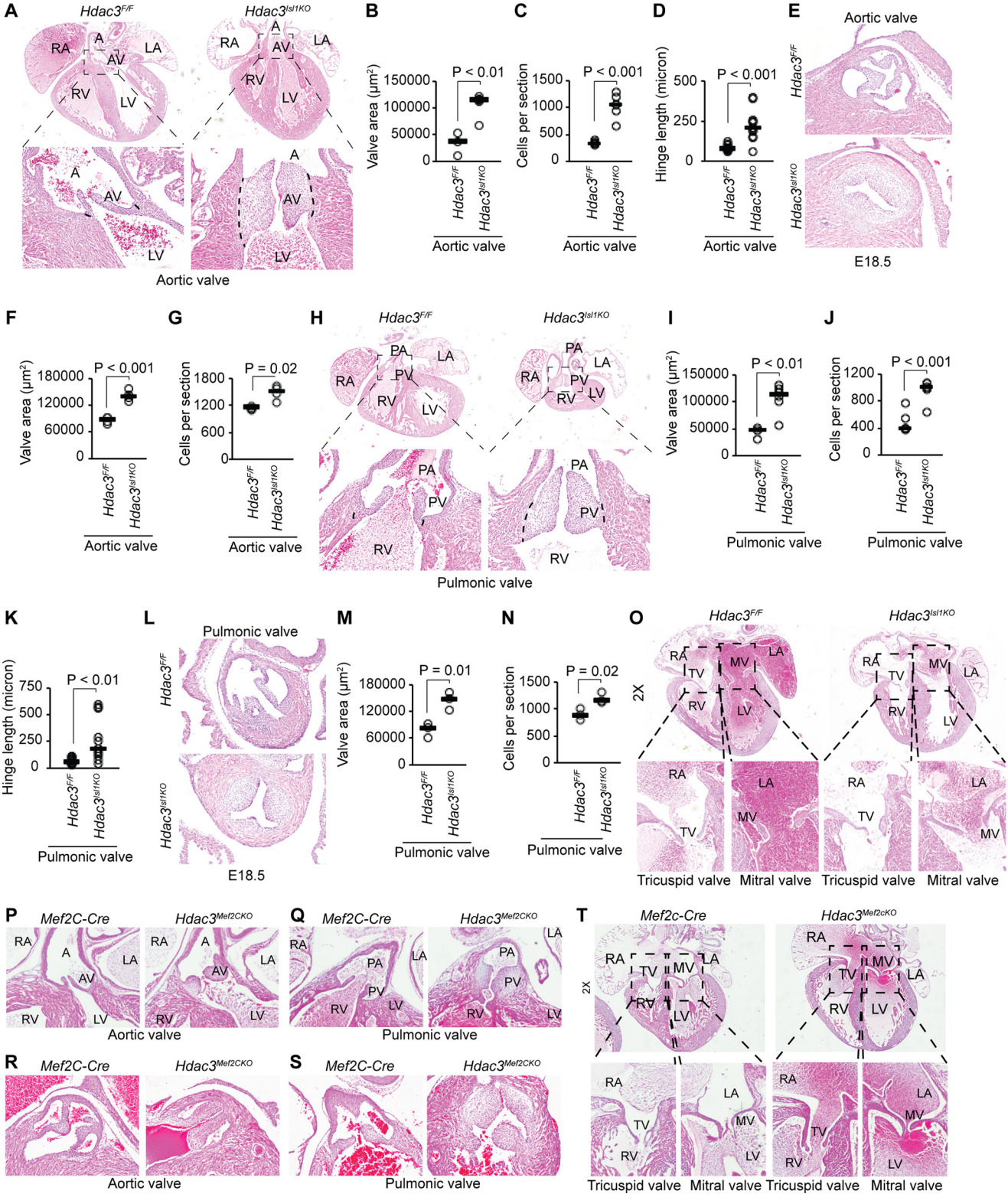

diomyocytes at E8.5 (64), did not reveal malrotation of outflow tract, overriding aorta, double outlet right ventricle, or valve defects observed in $Hdac3^{Isl1KO}$ or $Hdac3^{Mef2CKO}$ embryos (Fig. 6, *A*–*O*). Importantly, genetic deletion of *Hdac3* using *Tagln-Cre* ($Hdac3^{TaglnKO}$), which is expressed in differentiated mesenchymal or smooth muscle cells at E8.5 (65), recapitulated outflow tract malrotation, overriding aorta, double outlet right ventricle, aberrant semilunar valve development, membranous ventricular septal defect, disorganized collagen, and fragmented elastin in great vessel walls and showed hyperplastic semilunar valves with expanded proteoglycans and aberrant collagen deposition, as observed in $Hdac3^{Isl1KO}$ and $Hdac3^{Mef2CKO}$ embryos (Fig. 7, *A*–*L*). Expression of positive regulators of TGF-β pathway genes, smooth muscle markers, proteoglycans, and collagens were 4–20-fold up-regulated in $Hdac3^{TaglnKO}$ semilunar valves ($p < 0.03$; Fig. 7*M*). $Hdac3^{TaglnKO}$ outflow tract cushion explants displayed an ~3-fold increase in EndMT ($p < 0.03$) and ~20–40-fold expression changes in proteoglycans and smooth muscle genes ($p < 0.004$; Fig. 7, *N*–*Q*). Importantly, these changes were largely abolished by TGF-β-neutralizing antibody ($p < 0.004$), suggesting that aberrant EndMT and extracellular matrix remodeling in $Hdac3^{TaglnKO}$ hearts are mediated by TGF-β signaling (Fig. 7, *N*–*Q*). Together, these data suggest a primary role of HDAC3 in the second heart field-derived mesenchymal or smooth muscle cells during early cardiac development.

HDAC3 Epigenetically Silences TGF-β1 within Mesenchymal Cells by Recruiting EZH2 to the NCOR Complex—During EndMT, endothelial cells lose their endothelium-specific markers and morphology and acquire a mesenchymal cell-like phenotype (33). In this process, endothelium-derived mesenchymal cells displayed ~90% repression of TGF-β1 expression compared with endothelial cells ($p < 0.003$); however, this repression was completely absent in mesenchymal cells lacking HDAC3 (Fig. 8, *A* and *B*). We observed ~0.6–1.8% enrichment of HDAC3 at a regulatory region upstream of TGF-β1 within mesenchymal cells compared with endothelial cells ($p < 0.02$; Fig. 8, *C* and *D*). We evaluated chromatin occupancy of various histone marks to determine the regulatory mechanism of the HDAC3-enriched region upstream of TGF-β1 within mesenchymal cells. ChIP-qPCR analysis revealed loss of trimethylation of Lys-27 on histone H3 (H3K27me3) and ~8% enrichment of acetylation of Lys-27 on histone H3 (H3K27ac) at the TGF-β1 regulatory region in $Hdac3^{Isl1KO}$ semilunar valves compared with control ($p < 0.04$, Fig. 8, *E* and *F*). Consistent with these findings, $Hdac3^{Isl1KO}$ semilunar valves displayed ~0.9–3% enrichment of RNA polymerase II and CREBBP ($p < 0.006$) and abolished occupancy of EZH2, EED, and SUZ12, the H3K27 methyltransferase components of PRC2 complex, at the TGF-β1 regulatory region (Fig. 8, *G*–*K*). NCOR1 was required for recruitment of HDAC3 to the TGF-β1 locus (Fig. 8*L*). Interestingly, NCOR1 occupancy remained unchanged at this locus in $Hdac3^{Isl1KO}$ semilunar valves, suggesting that HDAC3 is not required for NCOR1 recruitment to the TGF-β1 regulatory region (Fig. 8*M*). Co-ChIP-qPCR analysis revealed co-occupancy of HDAC3 with either EZH2, H3K27me3, or NCOR1 at the TGF-β1 locus in wild-type semilunar valves (Fig. 8*N*). HDAC3 interacts with EZH2 within mesenchymal cells of semilunar valves (Fig. 8*O*). Importantly, EZH2 and NCOR1 are required for deposition of the H3K27me3 mark at the TGF-β1 locus within valvular mesenchymal cells (Fig. 8*P*). These data suggest that HDAC3 is required to mediate epigenetic silencing of TGF-β1 within mesenchymal cells of semilunar valves.

Deacetylase Activity of HDAC3 Is Dispensable for EndMT and Epigenetic Silencing of TGF-β1—Approximately 10% of mammalian enzymes are catalytically inactive (66). These "dead" enzymes or pseudoenzymes are biologically functional; however, their enzyme-independent functions remain largely undefined. A recent study (67) describes a deacetylase-independent function of HDAC3 in lipid metabolism. To determine whether deacetylase activity of HDAC3 is required to regulate EndMT, expression of *Tgf-β1*, and recruitment of EZH2 to the TGF-β1 locus, we generated a previously described mutant form of HDAC3 in which two highly conserved tandem His residues, 134 and 135, are mutated to alanine ($HDAC3^{H134A,H135A}$). These mutations do not affect its expression (Fig. 9, *A* and *B*), chromatin recruitment, and interaction with NCOR1 (67); however, they render HDAC3 completely inactive (Fig. 9*C*). HDAC3-null outflow tract cushion explants showed an ~2-fold increase in EndMT ($p < 0.05$), and these changes were largely rescued by either wild-type HDAC3 or $HDAC3^{H134A,H135A}$ expression ($p < 0.04$; Fig. 9, *D* and *E*). Similarly, either wild-type HDAC3 or $HDAC3^{H134A,H135A}$ rescued aberrant *Tgf-β1* transcription within cultured HDAC3-null semilunar valve mesenchymal cells ($p < 0.0004$; Fig. 9*F*). Hence, we generated a mutant TGF-β1 promoter luciferase reporter lacking the HDAC3 enriched regulatory region (−42 to −1 upstream of ATG).

FIGURE 2. **HDAC3 is required for semilunar valve development.** *A*, hematoxylin- and eosin-stained sections demonstrate thick, hyperplastic, and dysmorphic aortic valve in $Hdac3^{Isl1KO}$ E18.5 hearts. *B*, quantification of aortic valve area, measured from frontal sections of E18.5 hearts. *C*, quantification of number of nuclei per aortic valve section, counted from hematoxylin- and eosin-stained frontal sections of E18.5 hearts. *D*, quantification of width of junction between aortic valve and cardiac wall, measured from frontal sections of E18.5 hearts. *E*, hematoxylin- and eosin-stained sections demonstrate thick, hyperplastic, dysmorphic, and bicuspid aortic valve in $Hdac3^{Isl1KO}$ E18.5 hearts. *F*, quantification of aortic valve area, measured from cross-sections of E18.5 hearts. *G*, quantification of number of nuclei per aortic valve section, counted from hematoxylin- and eosin-stained cross-sections of E18.5 hearts. *H*, hematoxylin- and eosin-stained sections demonstrate thick, hyperplastic, and dysmorphic pulmonic valve in $Hdac3^{Isl1KO}$ E18.5 hearts. *I*, quantification of pulmonic valve area, measured from frontal sections of E18.5 hearts. *J*, quantification of number of nuclei per pulmonic valve section, counted from hematoxylin- and eosin-stained frontal sections of E18.5 hearts. *K*, width of hinge region in pulmonic valve measured from frontal sections of E18.5 hearts. *L*, hematoxylin- and eosin-stained sections demonstrate thick, hyperplastic, dysmorphic, and tricuspid pulmonic valve in $Hdac3^{Isl1KO}$ E18.5 hearts. *M*, quantification of pulmonic valve area, measured from cross-sections of E18.5 hearts. *N*, quantification of number of nuclei per pulmonic valve section, counted from hematoxylin- and eosin-stained cross-sections of E18.5 hearts. *O*, hematoxylin- and eosin-stained sections demonstrate normal tricuspid and mitral valve morphology in $Hdac3^{Isl1KO}$ E18.5 hearts. *P* and *Q*, hematoxylin- and eosin-stained sections show thickened, hyperplastic aortic (*P*) and pulmonic valves (*Q*) in E18.5 $Hdac3^{Mef2CKO}$ hearts. *R*, hematoxylin- and eosin-stained sections show hyperplastic, bicuspid aortic valve in E18.5 $Hdac3^{Mef2CKO}$ E18.5 hearts. *S*, hematoxylin- and eosin-stained sections show hyperplastic, tricuspid pulmonic valve in E18.5 $Hdac3^{Mef2CKO}$ hearts. *T*, hematoxylin- and eosin-stained sections demonstrate normal mitral and tricuspid valves in E18.5 $Hdac3^{Mef2CKO}$ hearts. *RA*, right atrium; *LA*, left atrium; *A*, aorta; *AV*, aortic valve; *PA*, pulmonary artery; *PV*, pulmonic valve; *RV*, right ventricle; *LV*, left ventricle; *MV*, mitral valve; *TV*, tricuspid valve.

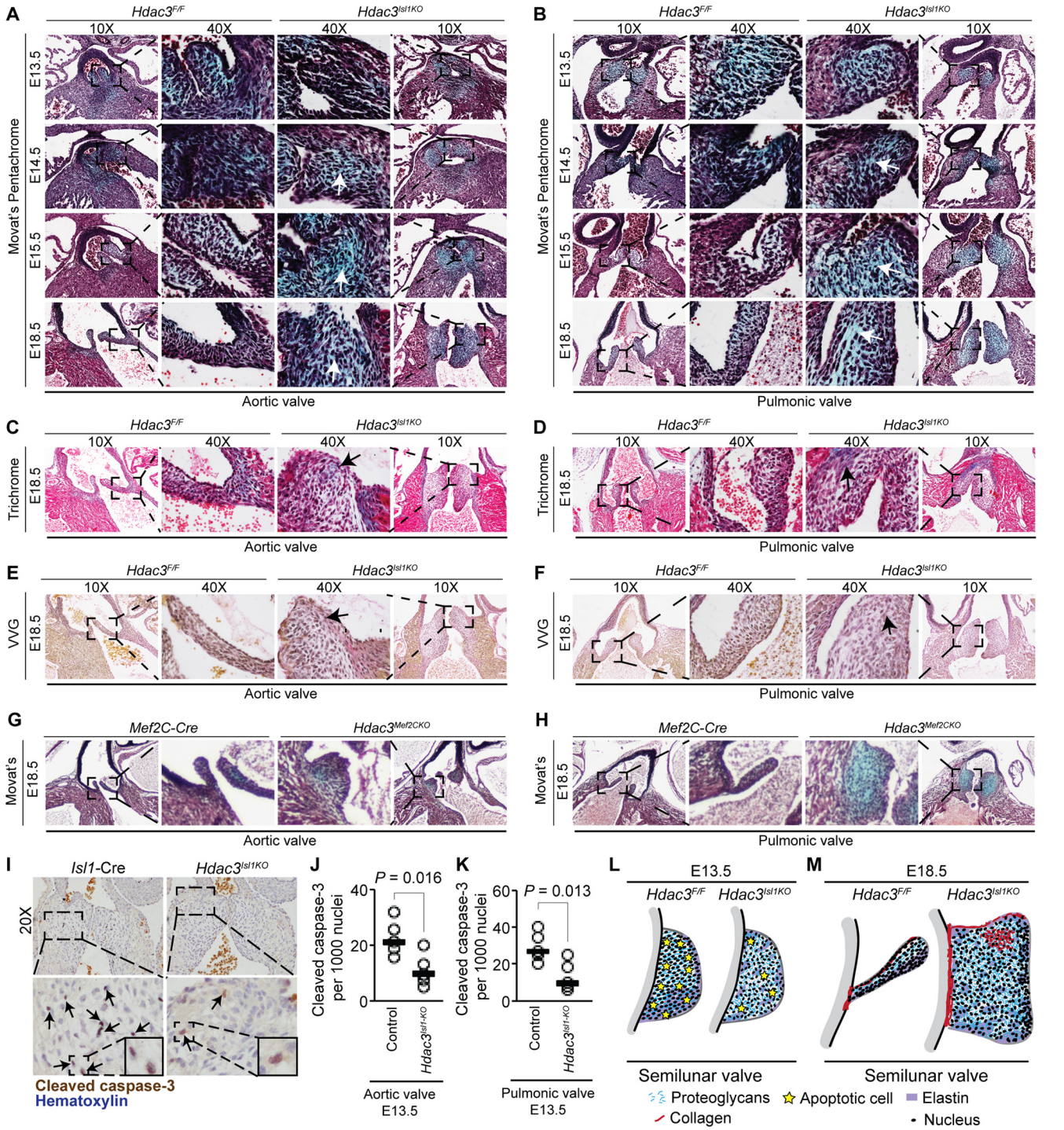

FIGURE 3. **HDAC3 is required for extracellular matrix homeostasis and remodeling of semilunar valves.** *A*, Movat's pentachrome staining of remodeling aortic valve shows an increase in proteoglycans (*arrows*, *blue*) from E13.5 to E18.5 in *Hdac3*^{Isl1KO} aortic valves with a reduction and remodeling of proteoglycans in control valves. *B*, Movat's pentachrome staining of remodeling pulmonic valve shows an increase in proteoglycans (*arrows*, *blue*) from E13.5 to E18.5 in *Hdac3*^{Isl1KO} pulmonic valves with a reduction and remodeling of proteoglycans in control valves. *C*, Masson's trichrome staining demonstrates disorganized collagen expression (*arrow*, *blue*) in *Hdac3*^{Isl1KO} E18.5 aortic valve. *D*, Masson's trichrome staining demonstrates disorganized collagen expression (*arrow*, *blue*) in *Hdac3*^{Isl1KO} E18.5 pulmonic valve. *E*, Verhoeff-Van Gieson (*VVG*) staining shows disorganized collagen expression (*arrow*, *red*) in *Hdac3*^{Isl1KO} E18.5 aortic valve. *F*, Verhoeff-Van Gieson staining shows disorganized collagen expression (*arrow*, *red*) in *Hdac3*^{Isl1KO} E18.5 aortic valve. *G*, Movat's pentachrome-stained sections show increased proteoglycans (*blue*) in aortic valve cusps of E18.5 *Hdac3*^{Mef2CKO} hearts. *H*, Movat's pentachrome staining reveals increased proteoglycans (*blue*) in E18.5 *Hdac3*^{Mef2CKO} pulmonic valve. *I*, representative images of cleaved caspase-3 immunostaining in E13.5 semilunar valves. *Arrows*, positive staining. *J*, quantification of cleaved caspase-3-positive cells in E13.5 control and *Hdac3*^{Isl1KO} aortic valves. *K*, quantification of cleaved caspase-3-positive cells in E13.5 control and *Hdac3*^{Isl1KO} pulmonic valves. *L*, schematic model depicting disorganized extracellular matrix and reduced apoptosis in *Hdac3*^{Isl1KO} E13.5 semilunar valves. *M*, schematic model showing hyperplastic, enlarged, and disorganized *Hdac3*^{Isl1KO} E18.5 semilunar valves.

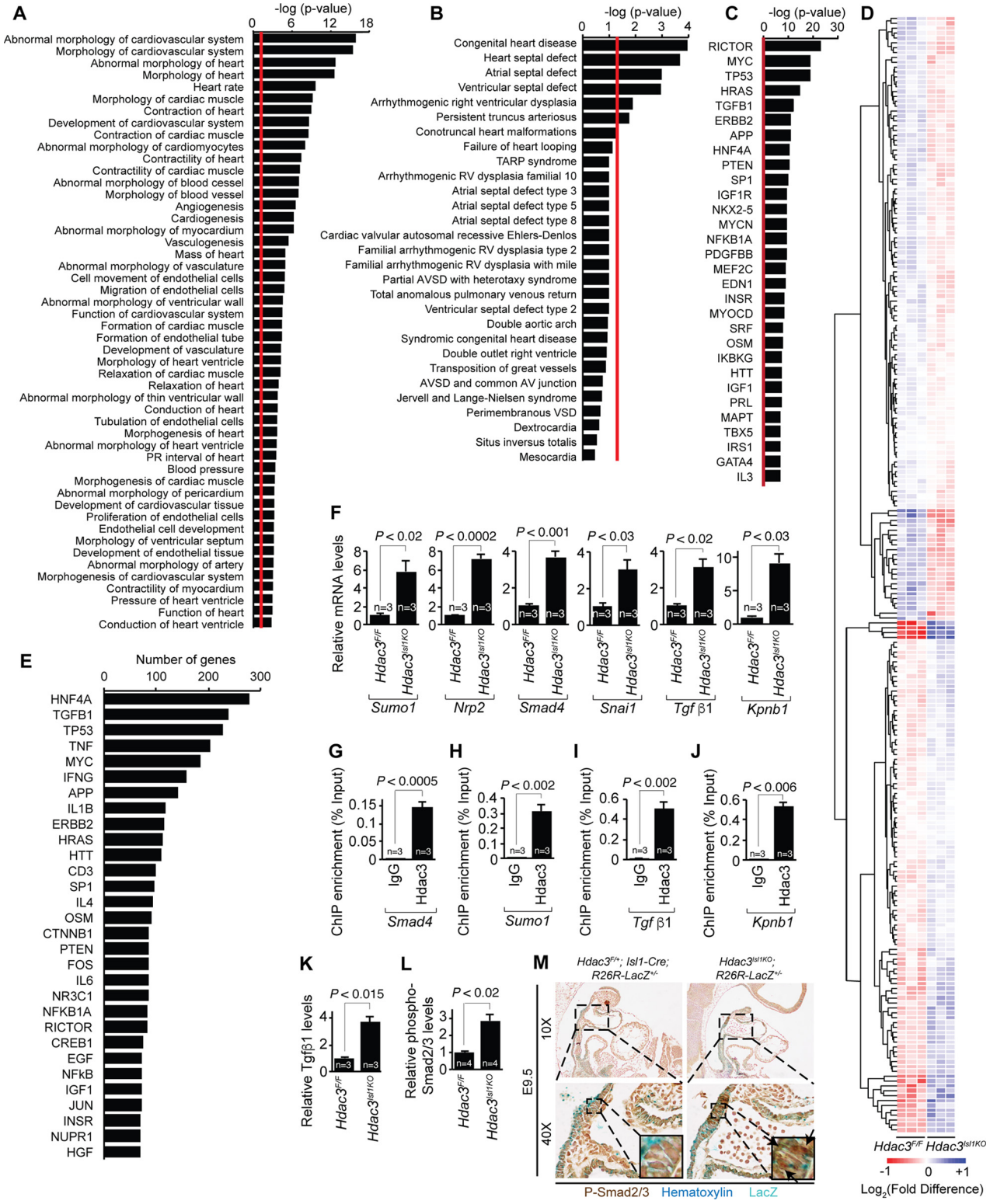

FIGURE 4. **HDAC3 is a critical regulator of TGF-β signaling pathway.** *A–E*, IPA of microarray data from E9.5 *Hdac3*^{Isl1KO} hearts. *A*, cardiovascular development and function subcategories significantly dysregulated in E9.5 *Hdac3*^{Isl1KO} hearts, sorted by significance, from IPA diseases and function analysis. *B*, classes of congenital heart anomalies affected in E9.5 *Hdac3*^{Isl1KO} hearts, sorted by significance, from IPA diseases and function analysis. *C*, 30 most significant upstream regulators from IPA upstream analysis of E9.5 *Hdac3*^{Isl1KO} microarray data. *D*, clustered heat map of differentially expressed genes related to upstream regulator TGF-β1 from IPA upstream analysis of *Hdac3*^{Isl1KO} microarray data. *E*, top 30 upstream regulators, based on number of associated genes differentially expressed in E9.5 *Hdac3*^{Isl1KO} hearts from IPA upstream analysis. *F*, transcripts for *Sumo1*, *Nrp2*, *Smad4*, *Snai1*, *Tgf-β1*, and *Kpnb1* were detected by real-time qPCR in *Hdac3*$^{F/F}$ and *Hdac3*^{Isl1KO} outflow tract with right ventricle derived from E9.5 embryos (mean ± S.E. (*error bars*), $n = 3$). *G–J*, ChIP-qPCR analysis of HDAC3 recruitment to promoter-proximal regions of TGF-β pathway genes performed in wild-type E9.5 outflow tract (mean ± S.E., $n = 3$). *K* and *L*, ELISA for TGF-β1 (*K*) and phospho-SMAD2/3 (*L*) was performed in *Hdac3*$^{F/F}$ and *Hdac3*^{Isl1KO} outflow tracts (mean ± S.E., $n = 3$ (*K*) and $n = 4$ (*L*)). *M*, phospho-SMAD2/3 immunostaining (*arrows*) in E9.5 *Hdac3*^{Isl1KO}; *R26R-LacZ*$^{+/-}$ hearts.

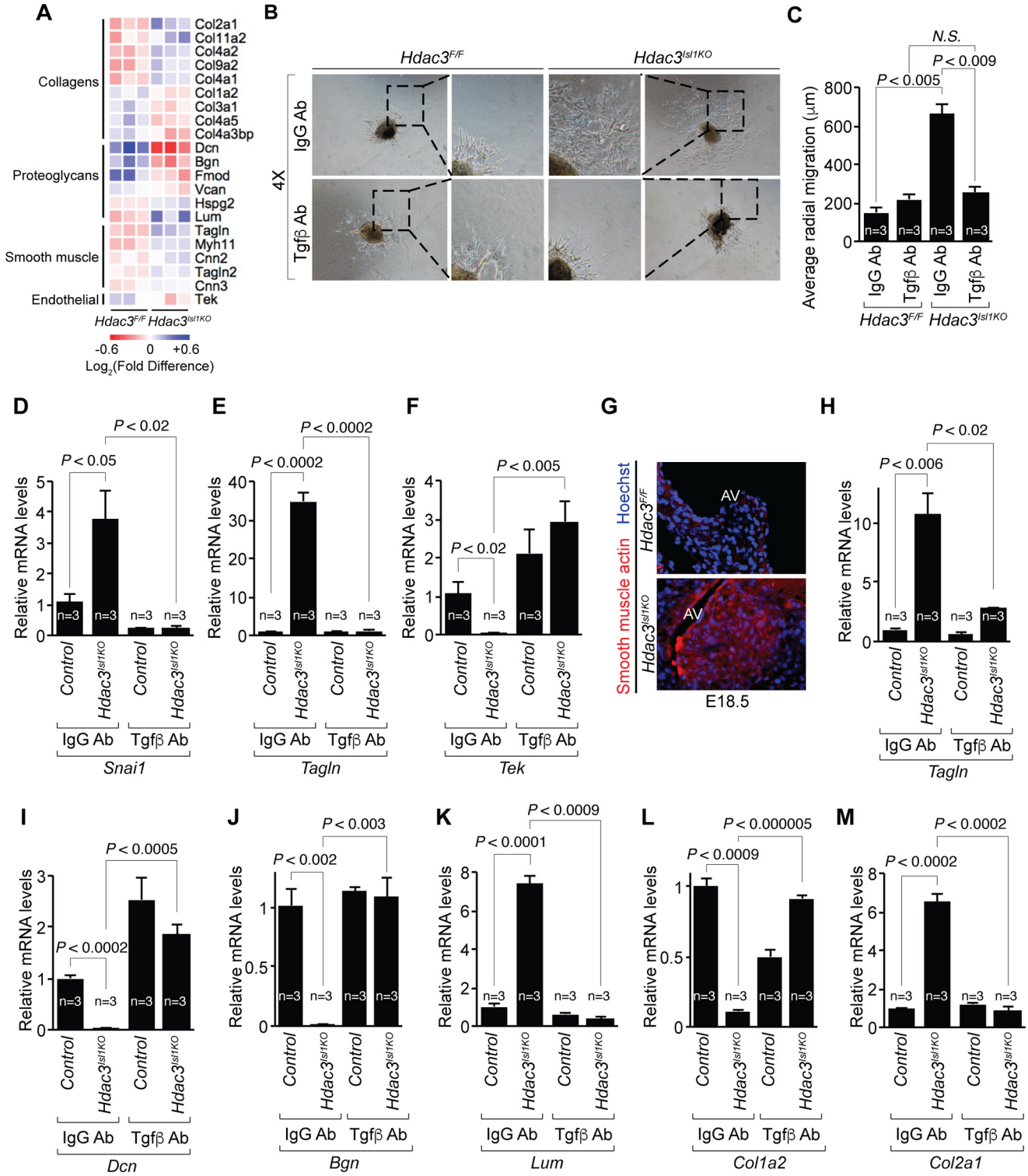

FIGURE 5. **TGF-β mediates aberrant expression of EndMT and extracellular matrix genes in *Hdac3*^{Isl1KO} heart.** *A*, heat map of microarray data shows differential expression of extracellular matrix, smooth muscle, and endothelium-related genes in *Hdac3*^{Isl1KO} E9.5 hearts. *B*, EndMT assay of TGF-β antibody-treated or IgG antibody-treated outflow tract cushion explants 24 h after isolation from *Hdac3*^{Isl1KO} and *Hdac3*$^{F/F}$ E10.5 hearts. *C*, quantification of average radial migration, measured in eight directions, from TGF-β antibody-treated or IgG antibody-treated outflow tract cushion explants from *Hdac3*^{Isl1KO} and *Hdac3*$^{F/F}$ E10.5 hearts, measured 24 h after isolation. *D–F*, transcripts for *Snai1* (*D*), *Tagln* (*E*), and *Tek* (*F*) were detected by real-time qPCR in IgG or TGF-β antibody-treated control and *Hdac3*^{Isl1KO} outflow tract explants derived from E9.5 hearts (mean ± S.E. (*error bars*), $n = 3$). *G*, immunostaining for smooth muscle actin in *Hdac3*^{Isl1KO} and control E18.5 aortic valves (*AV*). *H–M*, transcripts for *Tagln* (*H*), *Dcn* (*I*), *Bgn* (*J*), *Lum* (*K*), *Col1a2* (*L*), and *Col2a1* (*M*) were detected by real-time qPCR in IgG or TGF-β antibody-treated control and *Hdac3*^{Isl1KO} proximal outflow tract explants with semilunar valves derived from E14.5 embryos (mean ± S.E., $n = 3$).

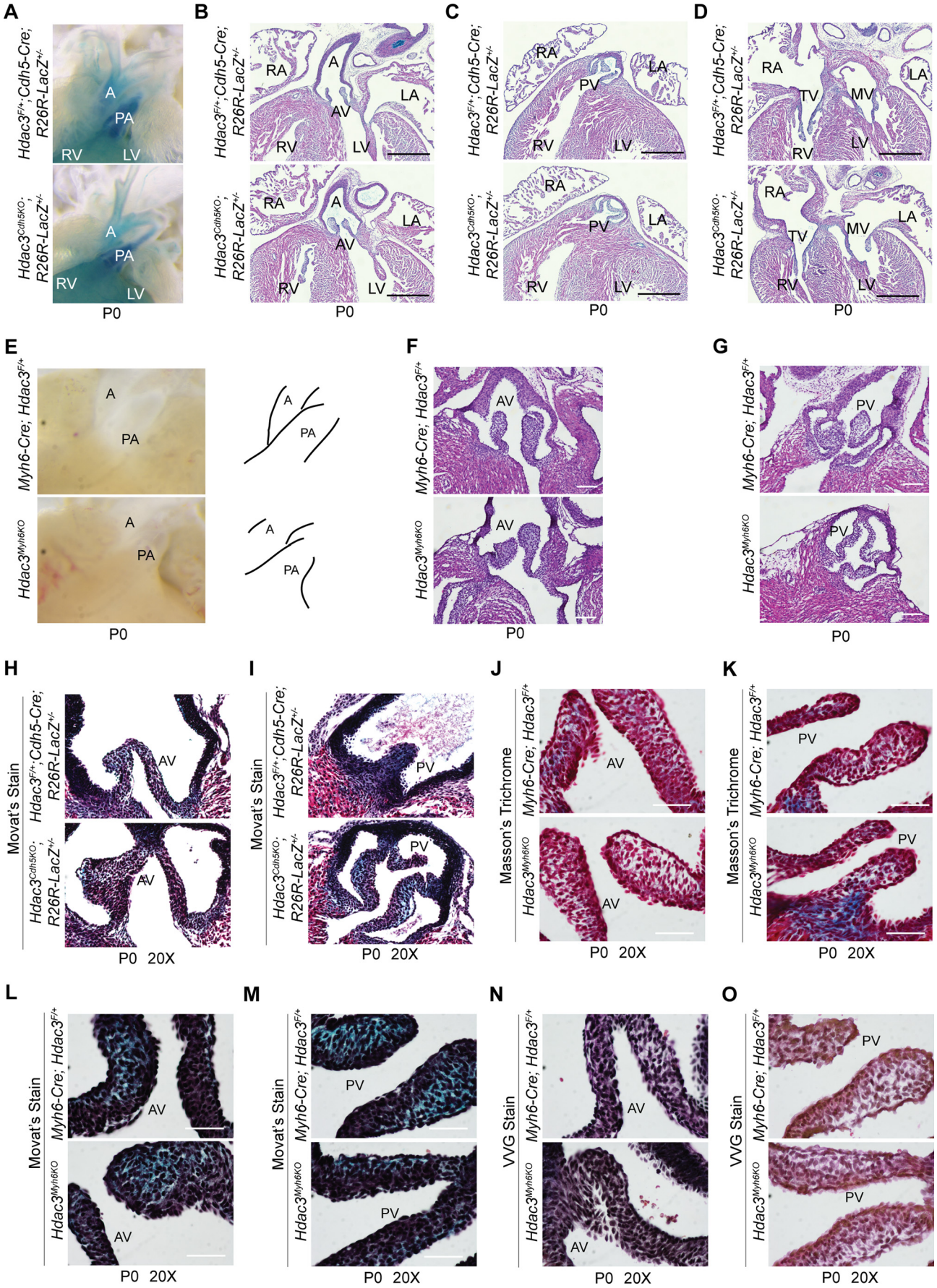
A
B
C
D
Hdac3F/+;Cdh5-Cre; R26R-LacZ+/-
Hdac3Cdh5KO; R26R-LacZ+/-
A
PA
RV
LV
RA
LA
AV
PV
TV
MV
P0
E
F
G
Myh6-Cre; Hdac3F/+
Hdac3Myh6KO
H
I
J
K
Movat's Stain
Masson's Trichrome
P0 20X
L
M
N
O
VVG Stain

Transfection of HDAC3 or HHDAC3^{H134A,H135A} resulted in ~90% repression of the wild-type TGF-β1 reporter ($p < 0.002$); however, it failed to repress the mutant TGF-β1 reporter (Fig. 9*G*). The mutant TGF-β1 promoter luciferase reporter displayed transcriptional activity similar to control (Fig. 9*G*). Interestingly, valvular mesenchymal cells expressing HDAC3^{H134A,H135A} showed similar levels of H3K27ac at the TGF-β1 locus compared with those expressing wild-type HDAC3, although HDAC3^{H134A,H135A} lacks the ability to actively deacetylate histones (Fig. 9*H*). Either wild-type HDAC3 or HDAC3^{H134A,H135A} expression restored chromatin occupancy of EZH2, EED, and SUZ12 and thereby deposition of the H3K27me3 mark at the TGF-β1 locus in cultured HDAC3-null semilunar valve mesenchymal cells (Fig. 9, *I–L*). Taken together, these findings demonstrate that HDAC3-mediated epigenetic silencing of TGF-β1 within second heart field-derived mesenchymal cells is essential for termination of EndMT (Fig. 10, *A* and *B*). In the absence of HDAC3, aberrant expression of TGF-β within mesenchymal cells leads to perpetual activation of mesenchymal cells to myofibroblasts, altered extracellular matrix homeostasis, and enhanced EndMT, which in turn, leads to congenital cardiac anomalies resembling those seen in patients with mutations causing activation of the TGF-β signaling pathway (Fig. 10, *A* and *B*).

Discussion

Previous studies from our group and others have demonstrated that HDACs are critical regulators of various developmental processes, including cardiogenesis (48, 49). Among class I HDACs (HDAC1, -2, -3, and -8), global loss of HDAC2 or HDAC8 in mice does not affect morphogenesis of second heart field-derived structures at birth (43, 45, 46). Interestingly, murine embryos lacking HDAC1 within the second heart field (*Hdac1*^{Isl1KO}) display normal cardiogenesis, including development of the outflow tract and semilunar valves.[3] Similarly, second heart field-derived structures appear normal in mice lacking class II HDACs, such as HDAC4, -5, -6, or -9 at birth (42). Taken together, our data reveal a unique and a specific role for HDAC3 in regulation of second heart field morphogenesis.

Second heart field progenitor cells progressively and restrictively differentiate into various cardiac cell types, including cardiomyocytes, endothelial cells, and mesenchymal or smooth muscle cells (3). Genetic ablation of HDAC3 in the second heart field progenitor cells using either *Isl1-Cre* or *Mef2c*-AHF-Cre resulted in ascending aortic dilatation, outflow tract malrotation, overriding aorta, double outlet right ventricle, semilunar valve stenosis, bicuspid aortic valve, and membranous ventricular septal defects that closely resembled those seen in patients with congenital cardiovascular diseases. Strikingly, genetic deletion of HDAC3 in mesenchymal or smooth muscle cells (*Hdac3*^{TaglnKO}) recapitulated the cardiovascular anomalies observed in *Hdac3*^{Isl1KO} and *Hdac3*^{Mef2CKO} embryos; however, genetic deletion of HDAC3 in differentiated cardiomyocytes (*Hdac3*^{Myh6KO}) or endothelial cells (*Hdac3*^{Cdh5KO}) did not recapitulate these defects. These observations define a spatiotemporal function of HDAC3 within mesenchymal or smooth muscle cells of second heart field-derived structures that is required for arterial pole morphogenesis (Fig. 10, *A* and *B*).

The anterior part of the second heart field contributes to the arterial pole of the heart, myocardial, and endothelial layers of the outflow tract, right ventricle, ventricular septum, and endocardial cushion mesenchyme of the outflow tract. The posterior part of the second heart field contributes to the venous pole of the heart, atria, dorsal mesenchymal protrusion, and atrial septum (4). *Isl1*^{Cre} marks both the anterior and posterior part of the second heart field (3). However, genetic deletion of ubiquitously expressed HDAC3 in the *Isl1*^{Cre} expression domain only affected morphogenesis of the anterior heart field-derived structures. Indeed, embryos lacking HDAC3 in the anterior second heart field (*Mef2C*-AHF-Cre) recapitulated these defects. Thus, HDAC3 mainly functions within the anterior part of the second heart field. Interestingly, embryos lacking HDAC3 in the second heart field display normal ventricular myocardium (data not shown). Previously, we demonstrated that HDAC3 is required in the primary heart field (*Nkx2-5* enhancer-Cre) for development of the ventricular myocardium at the early stages of cardiogenesis (48). Taken together, these findings suggest that once the primary heart field progenitors have adopted a cardiac fate to form the nascent heart tube, the second heart field-derived ventricular myocardium can develop independently of HDAC3. This is consistent with prior evidence that the ventricular myocardium remains unaffected after genetic manipulations or ablation of the second heart field progenitor cells (10, 11).

Outflow tract malrotation in tandem with ventricular septal defect is one of the most common cyanotic congenital heart defects at birth (13). Proper alignment, orientation, and septation of the cardiac outflow tract into the aorta and the pulmonary artery require intricate coordination and interaction among multiple cell types, including neural crest and second heart field (68). Cardiac neural crest cell-dependent processes, such as outflow tract septation and distal outflow tract morphogenesis, appeared normal in embryos lacking HDAC3 in the second heart field (Fig. 1*G*). Previously, we demonstrated that neural crest-specific genetic deletion of HDAC3 resulted in anomalous outflow tract septation and distal outflow tract mor-

[3] Z. Milstone and C. M. Trivedi, unpublished results.

FIGURE 6. **Endocardial or myocardial HDAC3 is dispensable for morphogenesis of second heart field-derived structures.** *A–D*, *Hdac3*^{Cdh5KO} hearts appear normal at birth. *A*, positions of aorta and pulmonary artery appear normal in *Hdac3*^{Cdh5KO} mice hearts at birth (P0). *B–D*, hematoxylin-, eosin-, and LacZ-stained sections of hearts from control and *Hdac3*^{Cdh5KO} mice. The aortic valve (*B*), pulmonic valve (*C*), tricuspid valve (*D*), and mitral valve (*D*) appear normal in size and shape in *Hdac3*^{Cdh5KO} hearts. *E–G*, *Hdac3*^{Myh6KO} hearts appear normal at birth. *E*, position of aorta and pulmonary artery appear normal in *Hdac3*^{Myh6KO} hearts at birth. *F* and *G*, hematoxylin- and eosin-stained sections of hearts from control and *Hdac3*^{Myh6KO} mice. Aortic valves (*F*) and pulmonic valves (*G*) appear normal in size and shape in *Hdac3*^{Myh6KO} hearts as compared with control. *H* and *I*, Movat's pentachrome staining show normal extracellular matrix organization in *Hdac3*^{Cdh5KO} P0 aortic valves (*H*) and pulmonic valves (*I*). *J–O*, *Hdac3*^{Myh6KO} extracellular matrix appears normal. Masson's trichrome staining of aortic valve (*J*) and pulmonic valve (*K*), Movat's pentachrome staining of aortic valve (*L*) and pulmonic valve (*M*), and Verhoeff-Van Gieson staining of aortic valve (*N*) and pulmonic valve (*O*) show normal extracellular matrix in semilunar valve cusps of P0 *Hdac3*^{Myh6KO} hearts. *A*, aorta; *PA*, pulmonary artery; *RA*, right atrium; *LA*, left atrium; *RV*, right ventricle; *LV*, left ventricle; *PV*, pulmonic valve; *AV*, aortic valve; *TV*, tricuspid valve; *MV*, mitral valve. *Scale bars*, 50 μm.

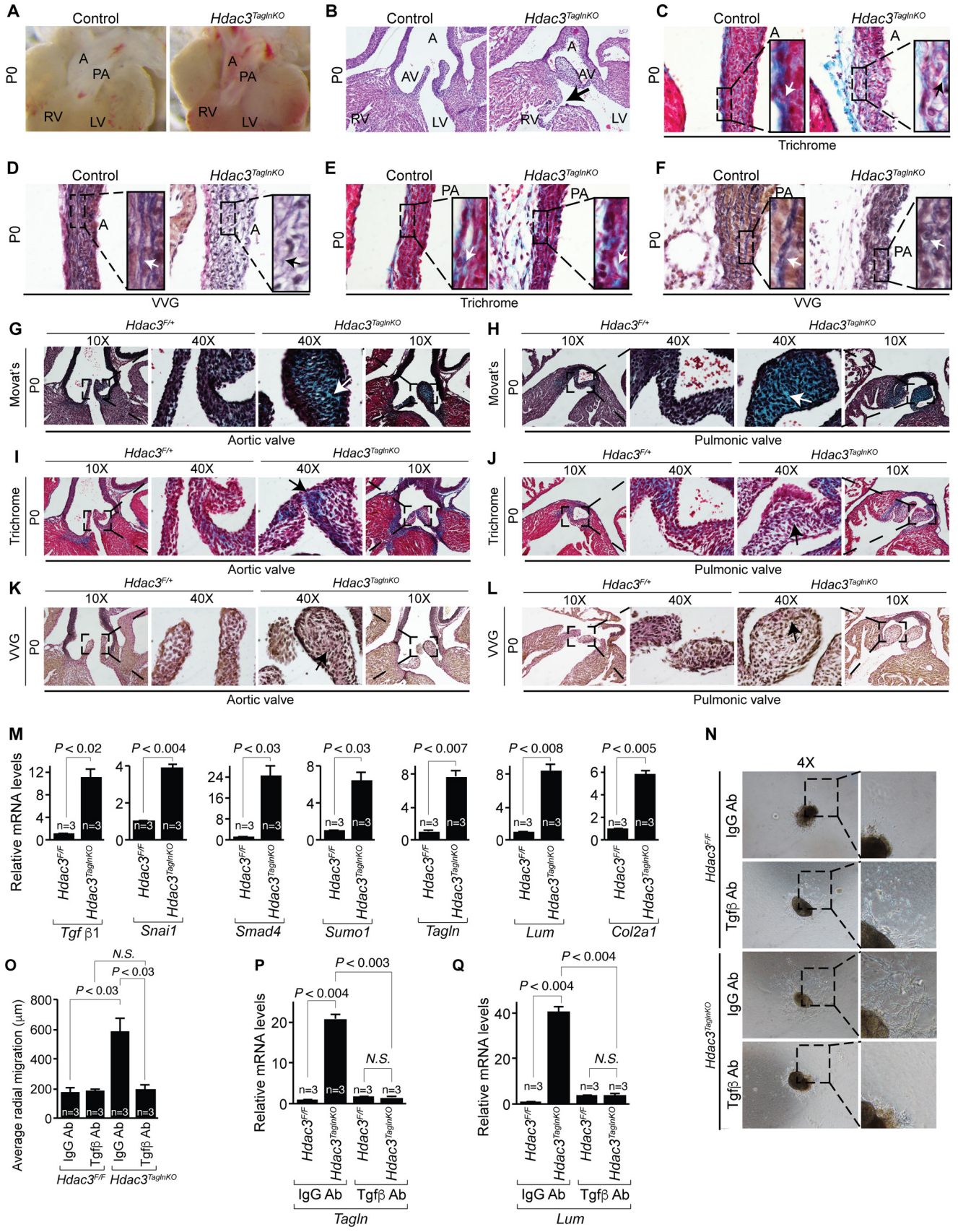
A
Control
Hdac3TaglnKO
P0
A
PA
RV
LV
B
AV
C
Trichrome
D
VVG
E
F
G
Hdac3F/+
10X
40X
Movat's
Aortic valve
H
Pulmonic valve
I
Trichrome
J
K
VVG
L
M
Relative mRNA levels
P < 0.02
P < 0.004
P < 0.03
P < 0.03
P < 0.007
P < 0.008
P < 0.005
n=3
Hdac3F/F
Hdac3TaglnKO
Tgf β1
Snai1
Smad4
Sumo1
Tagln
Lum
Col2a1
N
4X
IgG Ab
Tgfβ Ab
O
Average radial migration (μm)
N.S.
P < 0.03
P < 0.03
P
P < 0.003
P < 0.004
N.S.
Q
P < 0.004
P < 0.004
N.S.

phogenesis; however, outflow tract rotation and semilunar valve development were unaffected (69). Instead, second heart field-derived myocardium at the base of the outflow tract governs the normal outflow tract rotation (70). Prior studies also suggest that aberrant EndMT and remodeling of the outflow tract cushions give rise to structural outflow tract defects, particularly outflow tract malrotation (68). Our data establish that loss of HDAC3 triggers EndMT in the outflow tract cushion that can be markedly reduced by inhibiting TGF-β. Indeed, TGF-β and its downstream target genes are critical regulators of EndMT (17). In particular, TGF-β-activated SMAD proteins directly stimulate the expression of zinc finger transcription factor Snai1 within the outflow tract cushion (40). Studies in chicken and mice have shown that transcriptional repressor Snai1 is both sufficient and required for EndMT (71). Consistent with these findings, embryos lacking HDAC3 in the second heart field or valvular mesenchymal cells display a marked increase in Snai1 expression within the developing outflow tract and semilunar valves. Overall, our data demonstrate that genetic deletion of HDAC3 in the second heart field or in valvular mesenchymal cells augments TGF-β bioavailability, which, in turn, promotes aberrant EndMT and remodeling of the outflow tract cushion, and this, in part, may modulate outflow tract rotation. Importantly, our results highlight the underlying fact that outflow tract rotation and septation are independent processes regulated by distinct second heart field and cardiac neural crest lineages.

Our data reveal that HDAC3 is a critical regulator of extracellular matrix homeostasis within the second heart field-derived structures. Aberrant extracellular matrix is often an underlying pathology in semilunar valve stenosis, bicuspid aortic valve, and aortic dilatation (19, 38, 72). Patients with connective tissue disorders often exhibit altered composition and distribution of extracellular matrix within thickened semilunar valves and ascending aorta, resembling those seen in $Hdac3^{Isl1KO}$ and $Hdac3^{Mef2CKO}$ embryos. We demonstrate that HDAC3 is required to maintain proper composition of both proteoglycans and collagen in the developing semilunar valves and ascending aorta. The small leucine-rich proteoglycans, such as biglycan, decorin, and fibromodulin, sequester TGF-β to limit its bioavailability and thereby regulate proper remodeling of the hinge region of the semilunar valves and ascending aorta (37, 39). Without this sequestration, an increase of TGF-β bioavailability manifests as dilatation of ascending aorta, bicuspid aortic valves, and thickened semilunar valves in connective tissue disorders. Consistent with this model, our data demonstrate that genetic deletion of HDAC3 in the second heart field or valvular mesenchymal cells leads to significant down-regulation of biglycan, decorin, and fibromodulin, probably explaining increased TGF-β bioavailability, enlarged hinge region of semilunar valves, bicuspid aortic valves, and dilation of ascending aorta in $Hdac3^{Isl1KO}$ and $Hdac3^{Mef2CKO}$ embryos. Interestingly, we observed striking up-regulation of lumican, a small leucine-rich proteoglycan, in the outflow tract and developing semilunar valves of $Hdac3^{Isl1KO}$ embryos, probably explaining thickened semilunar valves. Patients with bicuspid aortic valve, the most common congenital heart defect, are at increased risk for ascending aortic dilatation (73). Proteoglycans facilitate collagen assembly and synthesis, a critical process for the development of semilunar valves and ascending aorta (37). Indeed, patients with mutations in collagen genes, such as *Col1a2* or *Col3a1*, are often predisposed to bicuspid aortic valves and aortic dilatation. Consistent with these observations, significantly reduced expression of *Col1a2* and *Col3a1* in $Hdac3^{Isl1KO}$ embryos might explain bicuspid aortic valves and ascending aortic dilatation.

Recent elegant studies (74) clearly demonstrate that in addition to their complex roles in early development, TGF-β signaling pathways are involved in many human diseases as a result of mutations in components of the pathways or aberrant regulation of signaling. Our study identifies HDAC3 as a novel and specific regulator of the TGF-β signaling pathway at the extracellular, membrane, cytoplasmic, and nuclear levels. For instance, our data demonstrate that loss of HDAC3 augments expression of extracellular agonist ligands of the TGF-β pathway, such as TGF-β1. Simultaneously, expression of extracellular antagonists of these ligands, such as decorin, biglycan, fibromodulin, and collagen, is strikingly diminished in the absence of HDAC3, probably explaining increased TGF-β bioavailability in $Hdac3^{Isl1KO}$ embryos. Similarly, gain of NRP2, SUMO1, KPNB1, and SMAD4 expression in $Hdac3^{Isl1KO}$ embryos would probably explain amplification of TGF-β signaling at the membrane, cytoplasmic, and nuclear levels.

FIGURE 7. **HDAC3 functions within mesenchymal or smooth muscle cells to regulate outflow tract and semilunar valve development.** *A*, dissected, fixed P0 hearts show malrotation of the aorta and pulmonary artery in $Hdac3^{TaglnKO}$ hearts. *B*, hematoxylin- and eosin-stained sections show double outlet right ventricle with aortic valve (*AV*) overriding a ventricular septal defect (*arrow*) in $Hdac3^{TaglnKO}$ P0 hearts. *C*, Masson's trichrome staining of P0 aortic vessel wall shows collagen on the outer surface of control aortic walls (*white arrow*, *blue staining*) and aberrant collagen expression throughout the vessel wall (*black arrow*, *blue staining*) in $Hdac3^{TaglnKO}$ aortic walls. *D*, Verhoeff-Van Gieson (*VVG*) staining of P0 aortic vessel wall shows thick, continuous elastin fibers (*white arrow*, *gray staining*) in control aortas and thin, fragmented elastin fibers (*black arrow*, *gray staining*) in $Hdac3^{TaglnKO}$ aortas. *E*, Masson's trichrome staining of P0 pulmonic artery wall shows collagen on the outer surface of control pulmonic artery walls (*white arrow*, *blue staining*) and aberrant collagen expression throughout the vessel wall (*white arrow*, *blue staining*) in $Hdac3^{TaglnKO}$ pulmonic artery walls. *F*, Verhoeff-Van Gieson staining of P0 pulmonic artery wall shows thick, continuous elastin fibers (*white arrow*, *gray staining*) in control aortas and thin, fragmented elastin fibers (*white arrow*, *gray staining*) in $Hdac3^{TaglnKO}$ pulmonic arteries. *G*, Movat's pentachrome staining of P0 aortic valve shows expanded proteoglycans (*arrow*, *blue*) in $Hdac3^{TaglnKO}$ aortic valve compared with $Hdac3^{F/+}$ control. *H*, Movat's pentachrome staining of P0 pulmonic valve shows expanded proteoglycans (*arrow*, *blue*) in $Hdac3^{TaglnKO}$ pulmonic valve compared with $Hdac3^{F/+}$ control. *I*, Masson's trichrome staining of P0 aortic valves shows disorganized collagen expression (*arrow*, *blue*) in $Hdac3^{TaglnKO}$ aortic valve. *J*, Masson's trichrome staining of P0 pulmonic valves shows disorganized collagen expression (*arrow*, *blue*) in $Hdac3^{TaglnKO}$ pulmonic valve. *K*, Verhoeff-Van Gieson stain of P0 aortic valves demonstrates disorganized collagen expression (*arrow*, *red*) in $Hdac3^{TaglnKO}$ aortic valve. *L*, Verhoeff-Van Gieson stain of P0 pulmonic valves demonstrates disorganized collagen expression (*arrow*, *red*) in $Hdac3^{TaglnKO}$ pulmonic valve. *M*, relative mRNA levels of *Tgf-β1*, *Snai1*, *Smad4*, *Sumo1*, *Tagln*, *Lum*, and *Col2a1* show increased expression in $Hdac3^{TaglnKO}$ E14.5 hearts. *N*, EndMT assay of TGF-β antibody-treated or IgG antibody-treated outflow tract cushion explants from $Hdac3^{TaglnKO}$ and $Hdac3^{F/F}$ E10.5 hearts, 24 h after isolation. *O*, quantification of average radial migration, measured in eight directions, from TGF-β antibody-treated or IgG antibody-treated outflow tract cushion explants from $Hdac3^{TaglnKO}$ and $Hdac3^{F/F}$ E10.5 hearts, measured 24 h after isolation. *P* and *Q*, transcripts for *Tagln* (*P*) and *Lum* (*Q*) were detected by real-time qPCR in IgG- or TGF-β antibody-treated control and $Hdac3^{TaglnKO}$ outflow tract cushion explants derived from E10.5 hearts (mean $\pm$ S.E. (*error bars*), $n = 3$).

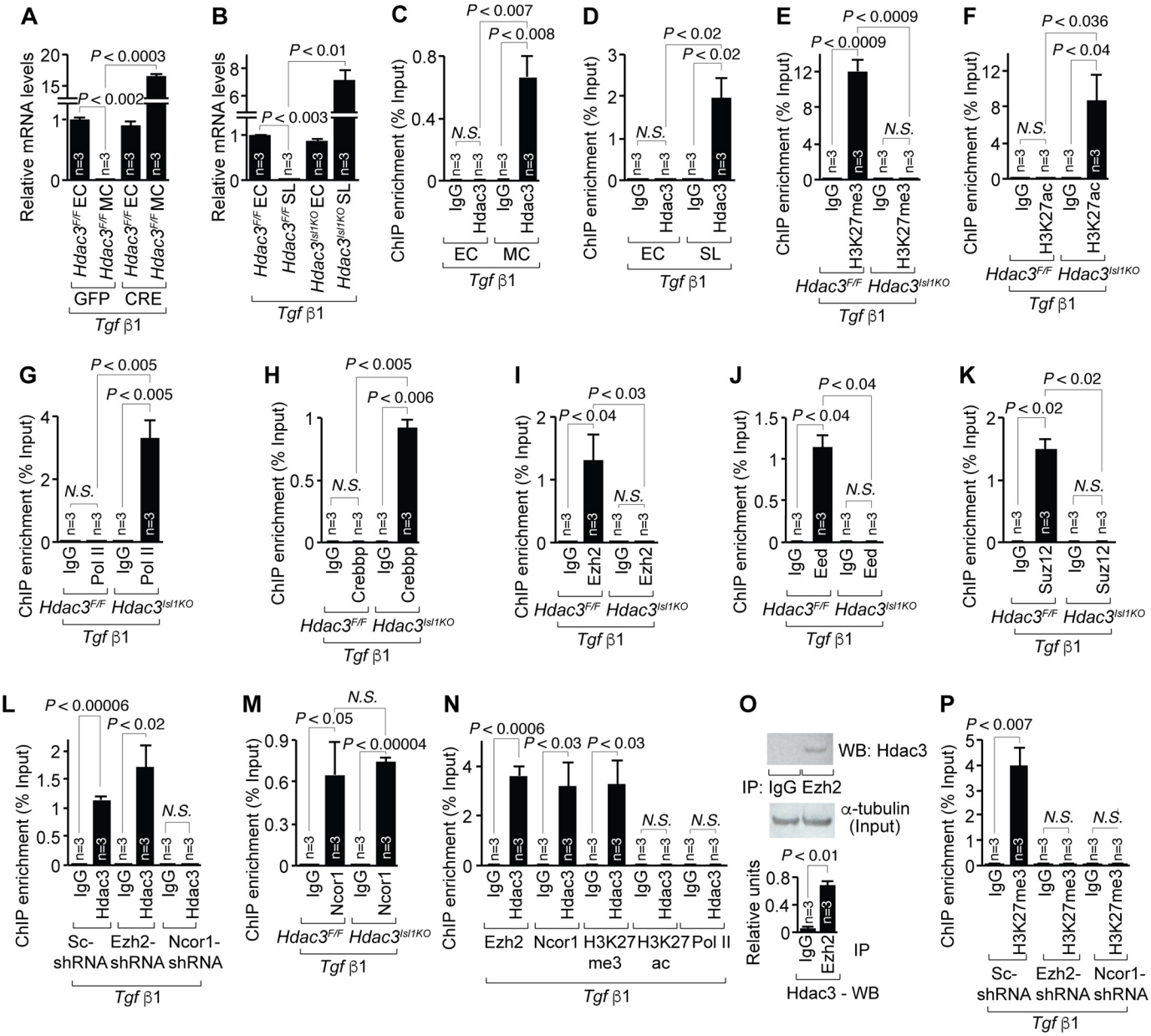

FIGURE 8. **HDAC3 epigenetically silences TGF-β1 within valvular mesenchymal cells by recruiting PRC2 complex to the NCOR complex.** *A*, relative mRNA levels of TGF-β1 in isolated cardiac endothelial cells (*EC*) or cardiac mesenchymal cells (*MC*) from E10.5 *Hdac3*$^{F/F}$ outflow tract cushion explants, infected either with CRE or GFP control lentivirus. *B*, relative mRNA levels of TGF-β1 in isolated cardiac endothelial cells or dissected semilunar valves (*SL*) derived from *Hdac3*^{Isl1KO} and *Hdac3*$^{F/F}$ E14.5 hearts. *C*, ChIP-qPCR analysis of HDAC3 occupancy upstream of TGF-β1 in isolated cardiac endothelial cells or cardiac mesenchymal cells from E10.5 outflow tract cushion explants. *D*, ChIP-qPCR analysis of HDAC3 occupancy upstream of TGF-β1 in isolated cardiac endothelial cells or dissected semilunar valves from E14.5 hearts. *E–K*, ChIP-qPCR analysis of H3K27 trimethylation (*E*), H3K27 acetylation (*F*), RNA polymerase II (*G*), CREBBP (*H*), EZH2 (*I*), EED (*J*), and SUZ12 (*K*) upstream of TGF-β1 in *Hdac3*^{Isl1KO} and control E14.5 semilunar valves. *L*, ChIP-qPCR analysis of HDAC3 occupancy upstream of TGF-β1 in E14.5 valvular mesenchymal cells infected with either control shRNA (*sc-shRNA*), EZH2 shRNA, or NCOR1 shRNA. *M*, ChIP-qPCR analysis of NCOR1 upstream of TGF-β1 in *Hdac3*^{Isl1KO} and control E14.5 semilunar valves. *N*, Co-ChIP for HDAC3 and either EZH2, NCOR1, H3K27me3, H3K27ac, or polymerase II upstream of TGF-β1 in E14.5 wild-type dissected semilunar valves. *O*, total lysates from E14.5 wild-type pooled semilunar valves were immunoprecipitated (*IP*) by EZH2 antibody, and Western blot was performed using HDAC3 antibody. α-Tubulin is shown as an input control. HDAC3 was quantified and normalized to total input α-tubulin using ImageJ software (mean $\pm$ S.E. (*error bars*), $n = 3$). *P*, ChIP-qPCR analysis of H3K27me3 upstream of TGF-β1 in E14.5 valvular mesenchymal cells infected with either control shRNA, EZH2 shRNA, or NCOR1 shRNA.

Our findings demonstrate that HDAC3 is required to maintain quiescence of valvular mesenchymal cells, the most prevalent cells of valvular cusps. Pathologic conditions promote activation and differentiation of valvular interstitial cells into myofibroblasts, smooth muscle-like fibroblasts that are observed in patients with semilunar valve disease (25). Myofibroblasts express smooth muscle-specific genes and secrete strikingly higher levels of TGF-β, proteoglycans, and collagen that alter the composition of the extracellular matrix (19). Hence, semilunar valve pathologies augment TGF-β bioavailability, which in turn promotes aberrant EndMT and transcriptional activation of smooth muscle and extracellular matrix genes within the myofibroblasts (24). TGF-β activation and aberrant extracellular matrix further promote the activation and differentiation of new valvular mesenchymal cells derived via EndMT (25). Consistent with these observations, our data dem-

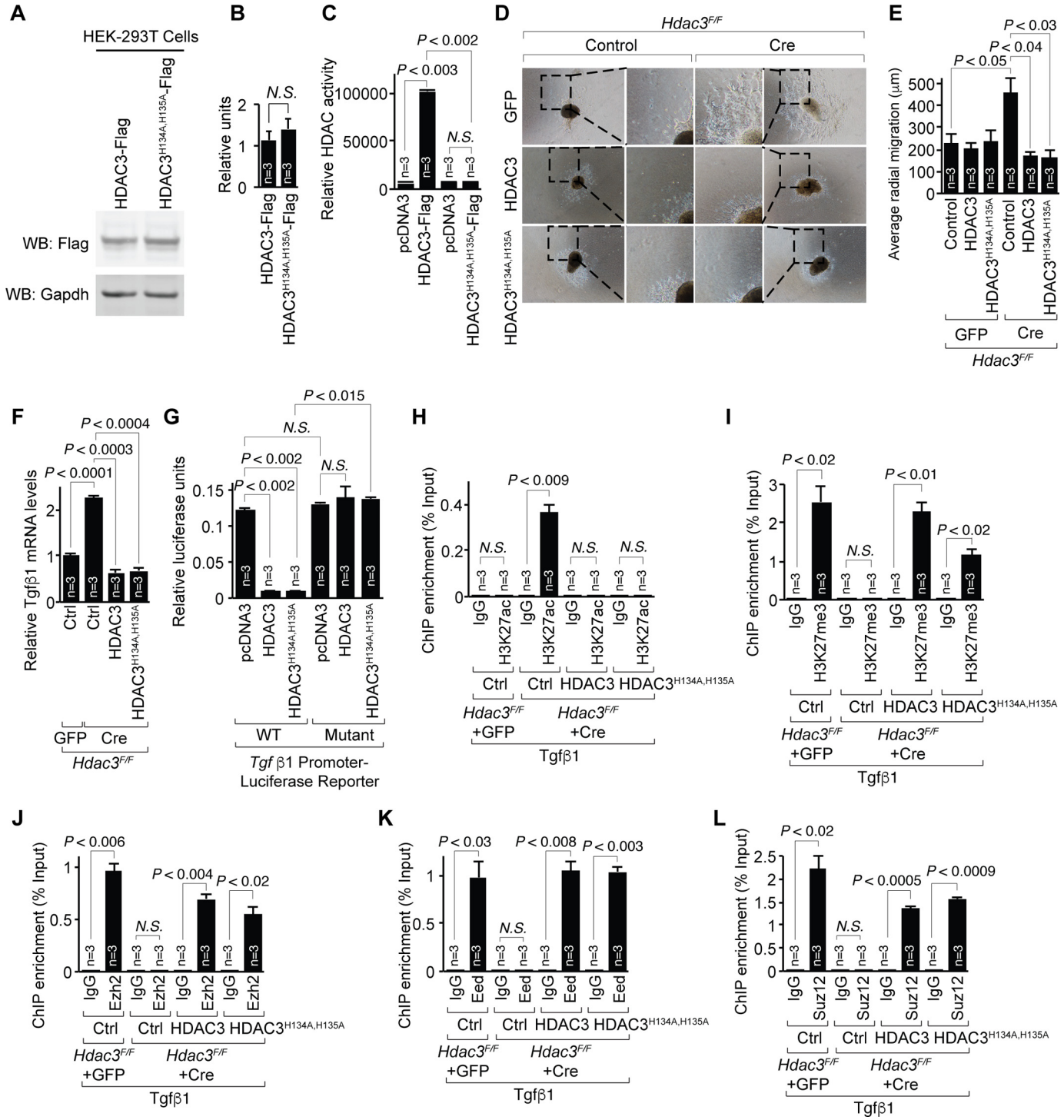

FIGURE 9. **HDAC3 functions in a deacetylase-independent manner to regulate EndMT and epigenetic silencing of TGF-β1.** *A*, HDAC3-FLAG and HDAC3^{H134A,H135A}-FLAG expression constructs were transfected in HEK-293T cells. Expression was detected by Western blot from whole cell lysates using FLAG antibody. GAPDH is shown as a loading control. *B*, HDAC3-FLAG and HDAC3^{H134A,H135A}-FLAG expression was quantified and normalized to total input GAPDH using ImageJ software (mean ± S.D. (*error bars*), $n = 3$). *C*, HDAC activity of HDAC3-FLAG and HDAC3^{H134A,H135A}-FLAG expression was quantified against a pseudosubstrate. *D*, EndMT assay of control- or Cre-infected E10.5 *Hdac3$^{F/F}$* outflow tract cushion explants co-infected with GFP, HDAC3-FLAG, or HDAC3^{H134A,H135A}-FLAG lentiviruses, imaged 24 h after isolation. *E*, quantification of average radial migration, measured in eight directions, of control- or Cre-infected E10.5 *Hdac3$^{F/F}$* outflow tract cushion explants co-infected with GFP, HDAC3-FLAG, or HDAC3^{H134A,H135A}-FLAG lentiviruses, measured 24 h after isolation (mean ± S.E. (*error bars*), $n = 3$). *F*, relative mRNA levels of *Tgf-β1* in control- or Cre-infected E14.5 *Hdac3$^{F/F}$* valvular mesenchymal cells co-infected with control, HDAC3-FLAG, or HDAC3^{H134A,H135A}-FLAG lentiviruses (mean ± S.E., $n = 3$). *G*, a 1309-bp TGF-β1 promoter luciferase reporter (*WT*) or a truncated, 1267-bp TGF-β1 promoter luciferase reporter, lacking an HDAC3-enriched region (mutant) were transfected in murine endothelial cells with and without an HDAC3-FLAG or HDAC3^{H134A,H135A}-FLAG expression plasmid. Induction is represented as a ratio of firefly and *Renilla* luciferase activity. *H–L*, ChIP-qPCR analysis of H3K27 acetylation (*H*), H3K27 trimethylation (*I*), EZH2 (*J*), EED (*K*), and SUZ12 (*L*) upstream of TGF-β1 in control- or Cre-infected E14.5 *Hdac3$^{F/F}$* valvular mesenchymal cells co-infected with control, HDAC3-FLAG, or HDAC3^{H134A,H135A}-FLAG lentiviruses (mean ± S.E., $n = 3$).

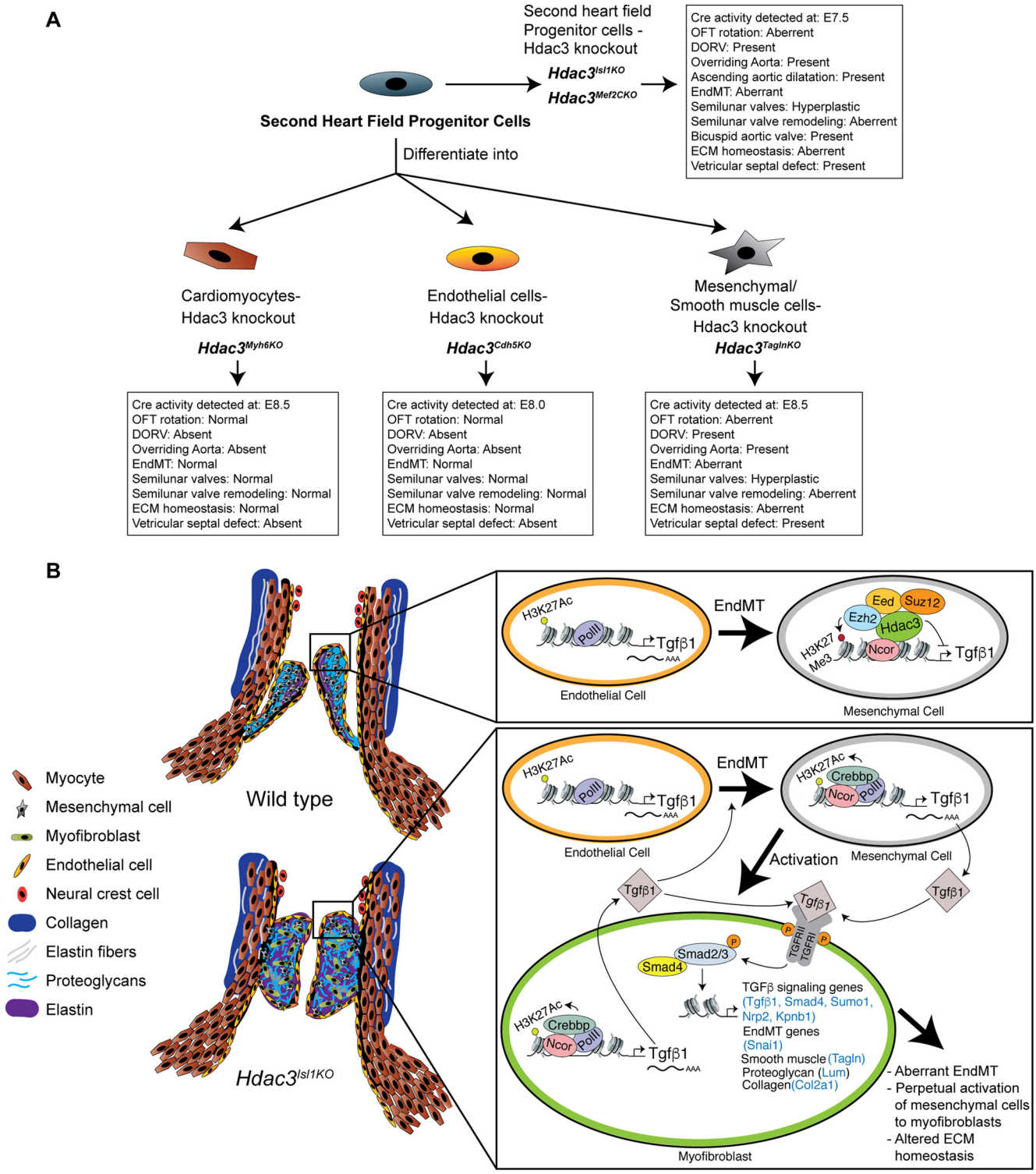

FIGURE 10. **Summary of phenotypes and proposed model of HDAC3 function within second heart field progenitor cells and second heart field-derived mesenchymal cells.** *A*, loss of HDAC3 in second heart field progenitor cells leads to outflow tract and semilunar valve pathologies. Strikingly, genetic deletion of HDAC3 in differentiated mesenchymal and smooth muscle cells (*Hdac3*^{TaglnKO}) recapitulates the majority of these phenotypes. However, deletion of HDAC3 in differentiated cardiomyocytes (*Hdac3*^{Myh6KO}) or endothelial cells (*Hdac3*^{Cdh5KO}) did not recapitulate the cardiovascular defects observed in *Hdac3*^{Isl1KO} embryos. *B*, *Hdac3*^{Isl1KO} hearts exhibit disorganized collagen and elastin within dilated aortic walls and hyperplastic semilunar valves containing activated myofibroblasts and disorganized extracellular matrix. In both control and *Hdac3*^{Isl1KO} cardiac endothelial cells, the upstream regulatory region of TGF-β1 is occupied by RNA polymerase II and CREBBP and exhibits H3K27 acetylation concomitant with TGF-β1 expression. In control semilunar valves, endothelial cells undergo EndMT to become mesenchymal cells. In these mesenchymal cells, NCOR1, HDAC3, and PRC2 complex (EZH2, EED, and SUZ12) are recruited to the upstream regulatory region of TGF-β1, which becomes trimethylated on histone H3 Lys-27, and TGF-β1 expression is epigenetically silenced. In *Hdac3*^{Isl1KO} hearts, EZH2, EED, and SUZ12 are not recruited to the TGF-β1 regulatory region, RNA polymerase II and CREBBP are present, and histone H3 Lys-27 remains acetylated, favoring aberrant expression of TGF-β1 in mesenchymal cells. TGF-β1 activates mesenchymal cells to become myofibroblasts, which perpetuate EndMT and activation of mesenchymal cells through continued induction of TGF-β1 and aberrant expression of extracellular matrix, including proteoglycans and collagen.

onstrate that loss of HDAC3 leads to strikingly higher expression of TGF-β1, smooth muscle genes, and aberrant expression of extracellular matrix genes within the valvular mesenchymal cells, and these changes were largely abolished by TGF-β-neutralizing antibody. Taken together, our findings support a model in which HDAC3-mediated repression of TGF-β1 within valvular mesenchymal cells is required to prevent perpetual activation of EndMT and to maintain extracellular matrix homeostasis in the semilunar valves.

Catalytically inactive enzymes or "pseudoenzymes" are clearly widespread, occurring in most enzyme families, including HDACs (66). For instance, class II HDACs, such as HDAC4, -5, -7, and -9, lack deacetylase activity due to a His substitution at the key Tyr residue (75). These pseudoenzymes function as scaffolding proteins to recruit various co-factors in a signal-dependent manner (42). Similarly, HDAC1 and -3, class I HDACs, and their deacetylase-dead mutants have the same degree of *in vivo* effect on cardiomyopathy (76). During endothelial-to-mesenchymal transition, epigenetic mechanisms regulating gene activation and silencing remain largely undefined (77). The present study provides the mechanistic basis of a deacetylase-independent function of HDAC3 as a scaffold to recruit methyltransferase components of PRC2 (polycomb repressive complex 2) to epigenetically silence TGF-β1. Repressor complex-mediated gene silencing is critical to maintain cellular identity of differentiated cells through multiple divisions (78). Recent evidence suggests that PRC2-mediated epigenetic silencing is maintained for many cell generations. EZH2, the major H3K27 methyltransferase of the PRC2 complex, supported by EED and SUZ12, catalyzes methylation of H3K27 to mediate chromatin compaction and thereby regulate differentiation and cell identity (79). Consistent with this model, our data demonstrate that HDAC3 recruits EZH2, EED, and SUZ12 to the NCOR complex in a deacetylase-independent manner and thereby mediates epigenetic silencing of TGF-β1 within valvular mesenchymal cells. In the absence of HDAC3, the NCOR complex fails to recruit PRC2 complex, resulting in aberrant recruitment of CREBBP, which catalyzes acetylation of H3K27 to mediate activation of TGF-β1 expression, which in turn promotes perpetual transdifferentiation of valvular mesenchymal cells to myofibroblasts. Subsequently, activated myofibroblasts secrete higher levels of extracellular matrix proteins and promote aberrant EndMT. Future investigations dissecting the modes of interaction among HDAC3, EZH2, EED, and SUZ12 will be important to determine PRC2-independent functions of HDAC3. Similarly, murine models expressing catalytically inactive HDAC3 would further define deacetylase-independent functions of HDAC3 during cardiogenesis.

Elucidation of the role of HDAC3 in the second heart field is directly relevant to human congenital heart disease. Marfan syndrome, Ehlers-Danlos syndrome, and Loeys-Dietz syndrome, caused by mutations and activation of TGF-β signaling genes, are associated with congenital cardiovascular anomalies resembling those seen in $Hdac3^{Isl1KO}$, $Hdac3^{Mef2CKO}$, or $Hdac3^{TaglnKO}$ embryos. Our data suggest that many of these cardiovascular defects, such as aortic dilatation, outflow tract defects, bicuspid aortic valve, semilunar valve stenosis, and membranous ventricular septal defects, are likely to be caused by defective morphogenesis of the second heart field and aberrant extracellular matrix as a result of anomalous epigenetic silencing of TGF-β.

Author Contributions—S. L. L., H. P. J., and C. M. T. designed, performed, and analyzed the experiments. S. L. L. and C. M. T. coordinated the study and wrote the paper. C. M. T. conceived the study, acquired funding, and supervised S. L. L. and H. P. J. All authors reviewed the results and approved the final version of the manuscript.

Acknowledgments—We gratefully acknowledge Dr. Sylvia Evans (University of California, San Diego) for providing Isl1-Cre mice, Dr. Brian Black (University of California, San Francisco) for providing Mef2C-AHF-Cre mice, and Dr. Mitchell Lazar (University of Pennsylvania) for providing $Hdac3^{Flox}$ mice. We thank the University of Massachusetts Medical School Genomics Core Facility for help with the microarray experiment.

References

1. Parker, S. E., Mai, C. T., Canfield, M. A., Rickard, R., Wang, Y., Meyer, R. E., Anderson, P., Mason, C. A., Collins, J. S., Kirby, R. S., Correa, A., and National Birth Defects Prevention Network (2010) Updated National Birth Prevalence estimates for selected birth defects in the United States, 2004–2006. *Birth Defects Res. A Clin. Mol. Teratol.* **88,** 1008–1016
2. Garcia-Martinez, V., and Schoenwolf, G. C. (1993) Primitive-streak origin of the cardiovascular system in avian embryos. *Dev. Biol.* **159,** 706–719
3. Evans, S. M., Yelon, D., Conlon, F. L., and Kirby, M. L. (2010) Myocardial lineage development. *Circ. Res.* **107,** 1428–1444
4. Buckingham, M., Meilhac, S., and Zaffran, S. (2005) Building the mammalian heart from two sources of myocardial cells. *Nat. Rev. Genet.* **6,** 826–835
5. Mjaatvedt, C. H., Nakaoka, T., Moreno-Rodriguez, R., Norris, R. A., Kern, M. J., Eisenberg, C. A., Turner, D., and Markwald, R. R. (2001) The outflow tract of the heart is recruited from a novel heart-forming field. *Dev. Biol.* **238,** 97–109
6. Waldo, K. L., Kumiski, D. H., Wallis, K. T., Stadt, H. A., Hutson, M. R., Platt, D. H., and Kirby, M. L. (2001) Conotruncal myocardium arises from a secondary heart field. *Development* **128,** 3179–3188
7. Verzi, M. P., McCulley, D. J., De Val, S., Dodou, E., and Black, B. L. (2005) The right ventricle, outflow tract, and ventricular septum comprise a restricted expression domain within the secondary/anterior heart field. *Dev. Biol.* **287,** 134–145
8. Kelly, R. G., Brown, N. A., and Buckingham, M. E. (2001) The arterial pole of the mouse heart forms from Fgf10-expressing cells in pharyngeal mesoderm. *Dev. Cell* **1,** 435–440
9. Cai, C.-L., Liang, X., Shi, Y., Chu, P.-H., Pfaff, S. L., Chen, J., and Evans, S. (2003) Isl1 identifies a cardiac progenitor population that proliferates prior to differentiation and contributes a majority of cells to the heart. *Dev. Cell* **5,** 877–889
10. McCulley, D. J., Kang, J.-O., Martin, J. F., and Black, B. L. (2008) BMP4 is required in the anterior heart field and its derivatives for endocardial cushion remodeling, outflow tract septation, and semilunar valve development. *Dev. Dyn.* **237,** 3200–3209
11. Ward, C., Stadt, H., Hutson, M., and Kirby, M. L. (2005) Ablation of the secondary heart field leads to tetralogy of Fallot and pulmonary atresia. *Dev. Biol.* **284,** 72–83
12. High, F. A., Jain, R., Stoller, J. Z., Antonucci, N. B., Lu, M. M., Loomes, K. M., Kaestner, K. H., Pear, W. S., and Epstein, J. A. (2009) Murine Jagged1/Notch signaling in the second heart field orchestrates Fgf8 expression and tissue-tissue interactions during outflow tract development. *J. Clin. Invest.* **119,** 1986–1996
13. van der Linde, D., Konings, E. E., Slager, M. A., Witsenburg, M., Helbing, W. A., Takkenberg, J. J., and Roos-Hesselink, J. W. (2011) Birth prevalence

of congenital heart disease worldwide: a systematic review and meta-analysis. *J. Am. Coll Cardiol.* **58,** 2241–2247
14. Kelly, R. G. (2012) The second heart field. *Curr. Top. Dev. Biol.* **100,** 33–65
15. Sanford, L. P., Ormsby, I., Gittenberger-de Groot, A. C., Sariola, H., Friedman, R., Boivin, G. P., Cardell, E. L., and Doetschman, T. (1997) TGFβ2 knockout mice have multiple developmental defects that are non-overlapping with other TGFβ knockout phenotypes. *Development* **124,** 2659–2670
16. Bartram, U., Molin, D. G., Wisse, L. J., Mohamad, A., Sanford, L. P., Doetschman, T., Speer, C. P., Poelmann, R. E., and Gittenberger-de Groot, A. C. (2001) Double-outlet right ventricle and overriding tricuspid valve reflect disturbances of looping, myocardialization, endocardial cushion differentiation, and apoptosis in TGF-β(2)-knockout mice. *Circulation* **103,** 2745–2752
17. Doetschman, T., Barnett, J. V., Runyan, R. B., Camenisch, T. D., Heimark, R. L., Granzier, H. L., Conway, S. J., and Azhar, M. (2012) Transforming growth factor β signaling in adult cardiovascular diseases and repair. *Cell Tissue Res.* **347,** 203–223
18. Lincoln, J., and Yutzey, K. E. K. (2011) Molecular and developmental mechanisms of congenital heart valve disease. *Birth Defects Res. A Clin. Mol. Teratol.* **91,** 526–534
19. Hinton, R. B., Jr., Lincoln, J., Deutsch, G. H., Osinska, H., Manning, P. B., Benson, D. W., and Yutzey, K. E. (2006) Extracellular matrix remodeling and organization in developing and diseased aortic valves. *Circ. Res.* **98,** 1431–1438
20. Lockhart, M., Wirrig, E., Phelps, A., and Wessels, A. (2011) Extracellular matrix and heart development. *Birth Defects Res. A Clin. Mol. Teratol.* **91,** 535–550
21. Waltenberger, J., Lundin, L., Oberg, K., Wilander, E., Miyazono, K., Heldin, C. H., and Funa, K. (1993) Involvement of transforming growth factor-β in the formation of fibrotic lesions in carcinoid heart disease. *Am. J. Pathol.* **142,** 71–78
22. Jian, B., Narula, N., Li, Q.-Y., Mohler, E. R., 3rd, and Levy, R. J. (2003) Progression of aortic valve stenosis: TGF-β1 is present in calcified aortic valve cusps and promotes aortic valve interstitial cell calcification via apoptosis. *Ann. Thorac. Surg.* **75,** 457–456; discussion 465–466
23. Fielitz, J., Hein, S., Mitrovic, V., Pregla, R., Zurbrügg, H. R., Warnecke, C., Schaper, J., Fleck, E., and Regitz-Zagrosek, V. (2001) Activation of the cardiac renin-angiotensin system and increased myocardial collagen expression in human aortic valve disease. *J. Am. Coll. Cardiol.* **37,** 1443–1449
24. Walker, G. A., Masters, K. S., Shah, D. N., Anseth, K. S., and Leinwand, L. A. (2004) Valvular myofibroblast activation by transforming growth factor-β: implications for pathological extracellular matrix remodeling in heart valve disease. *Circ. Res.* **95,** 253–260
25. Wang, H., Leinwand, L. A., and Anseth, K. S. (2014) Cardiac valve cells and their microenvironment: insights from *in vitro* studies. *Nat. Rev. Cardiol.* **11,** 715–727
26. Liu, A. C., and Gotlieb, A. I. (2008) Transforming growth factor-β regulates *in vitro* heart valve repair by activated valve interstitial cells. *Am. J. Pathol.* **173,** 1275–1285
27. Neptune, E. R., Frischmeyer, P. A., Arking, D. E., Myers, L., Bunton, T. E., Gayraud, B., Ramirez, F., Sakai, L. Y., and Dietz, H. C. (2003) Dysregulation of TGF-β activation contributes to pathogenesis in Marfan syndrome. *Nat. Genet.* **33,** 407–411
28. Loeys, B. L., Chen, J., Neptune, E. R., Judge, D. P., Podowski, M., Holm, T., Meyers, J., Leitch, C. C., Katsanis, N., Sharifi, N., Xu, F. L., Myers, L. A., Spevak, P. J., Cameron, D. E., De Backer, J., Hellemans, J., Chen, Y., Davis, E. C., Webb, C. L., Kress, W., Coucke, P., Rifkin, D. B., De Paepe, A. M., and Dietz, H. C. (2005) A syndrome of altered cardiovascular, craniofacial, neurocognitive and skeletal development caused by mutations in TGFBR1 or TGFBR2. *Nat. Genet.* **37,** 275–281
29. Morissette, R., Schoenhoff, F., Xu, Z., Shilane, D. A., Griswold, B. F., Chen, W., Yang, J., Zhu, J., Fert-Bober, J., Sloper, L., Lehman, J., Commins, N., Van Eyk, J. E., and McDonnell, N. B. (2014) Transforming growth factor-β and inflammation in vascular (type IV) Ehlers-Danlos syndrome. *Circ. Cardiovasc. Genet.* **7,** 80–88
30. Leier, C. V., Call, T. D., Fulkerson, P. K., and Wooley, C. F. (1980) The spectrum of cardiac defects in the Ehlers-Danlos syndrome, types I and III. *Ann. Intern. Med.* **92,** 171–178
31. Buntinx, I. M., Willems, P. J., Spitaels, S. E., Van Reempst, P. J., De Paepe, A. M., and Dumon, J. E. (1991) Neonatal Marfan syndrome with congenital arachnodactyly, flexion contractures, and severe cardiac valve insufficiency. *J. Med. Genet.* **28,** 267–273
32. MacCarrick, G., Black, J. H., 3rd, Bowdin, S., El-Hamamsy, I., Frischmeyer-Guerrerio, P. A., Guerrerio, A. L., Sponseller, P. D., Loeys, B., and Dietz, H. C., 3rd (2014) Loeys-Dietz syndrome: a primer for diagnosis and management. *Genet. Med.* **16,** 576–587
33. Massagué, J. (2012) TGFβ signalling in context. *Nat. Rev. Mol. Cell Biol.* **13,** 616–630
34. Yamaguchi, Y., Mann, D. M., and Ruoslahti, E. (1990) Negative regulation of transforming growth factor-β by the proteoglycan decorin. *Nature* **346,** 281–284
35. Corsi, A., Xu, T., Chen, X. D., Boyde, A., Liang, J., Mankani, M., Sommer, B., Iozzo, R. V., Eichstetter, I., Robey, P. G., Bianco, P., and Young, M. F. (2002) Phenotypic effects of biglycan deficiency are linked to collagen fibril abnormalities, are synergized by decorin deficiency, and mimic Ehlers-Danlos-like changes in bone and other connective tissues. *J. Bone Miner. Res.* **17,** 1180–1189
36. Danielson, K. G., Baribault, H., Holmes, D. F., Graham, H., Kadler, K. E., and Iozzo, R. V. (1997) Targeted disruption of decorin leads to abnormal collagen fibril morphology and skin fragility. *J. Cell Biol.* **136,** 729–743
37. Jepsen, K. J., Wu, F., Peragallo, J. H., Paul, J., Roberts, L., Ezura, Y., Oldberg, A., Birk, D. E., and Chakravarti, S. (2002) A syndrome of joint laxity and impaired tendon integrity in lumican- and fibromodulin-deficient mice. *J. Biol. Chem.* **277,** 35532–35540
38. Pulkkinen, L., Kainulainen, K., Krusius, T., Mäkinen, P., Schollin, J., Gustavsson, K. H., and Peltonen, L. (1990) Deficient expression of the gene coding for decorin in a lethal form of Marfan syndrome. *J. Biol. Chem.* **265,** 17780–17785
39. Dupuis, L. E., and Kern, C. B. (2014) Small leucine-rich proteoglycans exhibit unique spatiotemporal expression profiles during cardiac valve development. *Dev. Dyn.* **243,** 601–611
40. Vincent, T., Neve, E. P. A., Johnson, J. R., Kukalev, A., Rojo, F., Albanell, J., Pietras, K., Virtanen, I., Philipson, L., Leopold, P. L., Crystal, R. G., de Herreros, A. G., Moustakas, A., Pettersson, R. F., and Fuxe, J. (2009) A SNAIL1-SMAD3/4 transcriptional repressor complex promotes TGF-β mediated epithelial-mesenchymal transition. *Nat. Cell Biol.* **11,** 943–950
41. Yang, X.-J., and Seto, E. (2008) The Rpd3/Hda1 family of lysine deacetylases: from bacteria and yeast to mice and men. *Nat. Rev. Mol. Cell Biol.* **9,** 206–218
42. Haberland, M., Montgomery, R. L., and Olson, E. N. (2009) The many roles of histone deacetylases in development and physiology: implications for disease and therapy. *Nat. Rev. Genet.* **10,** 32–42
43. Trivedi, C. M., Luo, Y., Yin, Z., Zhang, M., Zhu, W., Wang, T., Floss, T., Goettlicher, M., Noppinger, P. R., Wurst, W., Ferrari, V. A., Abrams, C. S., Gruber, P. J., and Epstein, J. A. (2007) Hdac2 regulates the cardiac hypertrophic response by modulating Gsk3 β activity. *Nat. Med.* **13,** 324–331
44. Montgomery, R. L., Hsieh, J., Barbosa, A. C., Richardson, J. A., and Olson, E. N. (2009) Histone deacetylases 1 and 2 control the progression of neural precursors to neurons during brain development. *Proc. Natl. Acad. Sci. U.S.A.* **106,** 7876–7881
45. Haberland, M., Mokalled, M. H., Montgomery, R. L., and Olson, E. N. (2009) Epigenetic control of skull morphogenesis by histone deacetylase 8. *Genes Dev.* **23,** 1625–1630
46. Trivedi, C. M., Zhu, W., Wang, Q., Jia, C., Kee, H. J., Li, L., Hannenhalli, S., and Epstein, J. A. (2010) Hopx and Hdac2 interact to modulate Gata4 acetylation and embryonic cardiac myocyte proliferation. *Dev. Cell* **19,** 450–459
47. Trivedi, C. M., Lu, M. M., Wang, Q., and Epstein, J. A. (2008) Transgenic overexpression of Hdac3 in the heart produces increased postnatal cardiac myocyte proliferation but does not induce hypertrophy. *J. Biol. Chem.* **283,** 26484–26489
48. Lewandowski, S. L., Janardhan, H. P., Smee, K. M., Bachman, M., Sun, Z., Lazar, M. A., and Trivedi, C. M. (2014) Histone deacetylase 3 modulates Tbx5 activity to regulate early cardiogenesis. *Hum. Mol. Genet.* **23,** 3801–3809

49. Montgomery, R. L., Davis, C. A., Potthoff, M. J., Haberland, M., Fielitz, J., Qi, X., Hill, J. A., Richardson, J. A., and Olson, E. N. (2007) Histone deacetylases 1 and 2 redundantly regulate cardiac morphogenesis, growth, and contractility. *Genes Dev.* **21,** 1790–1802
50. Yang, L., Cai, C.-L., Lin, L., Qyang, Y., Chung, C., Monteiro, R. M., Mummery, C. L., Fishman, G. I., Cogen, A., and Evans, S. (2006) Isl1Cre reveals a common Bmp pathway in heart and limb development. *Development* **133,** 1575–1585
51. Mullican, S. E., Gaddis, C. A., Alenghat, T., Nair, M. G., Giacomin, P. R., Everett, L. J., Feng, D., Steger, D. J., Schug, J., Artis, D., and Lazar, M. A. (2011) Histone deacetylase 3 is an epigenomic brake in macrophage alternative activation. *Genes Dev.* **25,** 2480–2488
52. Alva, J. A., Zovein, A. C., Monvoisin, A., Murphy, T., Salazar, A., Harvey, N. L., Carmeliet, P., and Iruela-Arispe, M. L. (2006) VE-Cadherin-Cre-recombinase transgenic mouse: a tool for lineage analysis and gene deletion in endothelial cells. *Dev. Dyn.* **235,** 759–767
53. Carvalho, B. S., and Irizarry, R. A. (2010) A framework for oligonucleotide microarray preprocessing. *Bioinformatics* **26,** 2363–2367
54. Gentleman, R. C., Carey, V. J., Bates, D. M., Bolstad, B., Dettling, M., Dudoit, S., Ellis, B., Gautier, L., Ge, Y., Gentry, J., Hornik, K., Hothorn, T., Huber, W., Iacus, S., Irizarry, R., Leisch, F., Li, C., Maechler, M., Rossini, A. J., Sawitzki, G., Smith, C., Smyth, G., Tierney, L., Yang, J. Y. H., and Zhang, J. (2004) Bioconductor: open software development for computational biology and bioinformatics. *Genome Biol.* **5,** R80
55. R Core Team (2012) *R: a language and environment for statistical computing*. R Foundation for Statistical Computing, Vienna, Austria
56. Kolde, R. (2013) *pheatmap: Pretty Heatmaps*. R package version 0.7.7, R Foundation for Statistical Computing, Vienna, Austria
57. Lakkis, M. M., and Epstein, J. A. (1998) Neurofibromin modulation of ras activity is required for normal endocardial-mesenchymal transformation in the developing heart. *Development* **125,** 4359–4367
58. Yamamura, H., Zhang, M., Markwald, R. R., and Mjaatvedt, C. H. (1997) A heart segmental defect in the anterior-posterior axis of a transgenic mutant mouse. *Dev. Biol.* **186,** 58–72
59. Bhaskara, S., Chyla, B. J., Amann, J. M., Knutson, S. K., Cortez, D., Sun, Z.-W., and Hiebert, S. W. (2008) Deletion of histone deacetylase 3 reveals critical roles in S phase progression and DNA damage control. *Mol. Cell* **30,** 61–72
60. Montgomery, R. L., Potthoff, M. J., Haberland, M., Qi, X., Matsuzaki, S., Humphries, K. M., Richardson, J. A., Bassel-Duby, R., and Olson, E. N. (2008) Maintenance of cardiac energy metabolism by histone deacetylase 3 in mice. *J. Clin. Invest.* **118,** 3588–3597
61. Hinton, R. B., and Yutzey, K. E. (2011) Heart valve structure and function in development and disease. *Annu. Rev. Physiol.* **73,** 29–46
62. Sun, Y., Liang, X., Najafi, N., Cass, M., Lin, L., Cai, C.-L., Chen, J., and Evans, S. M. (2007) Islet 1 is expressed in distinct cardiovascular lineages, including pacemaker and coronary vascular cells. *Dev. Biol.* **304,** 286–296
63. Moretti, A., Caron, L., Nakano, A., Lam, J. T., Bernshausen, A., Chen, Y., Qyang, Y., Bu, L., Sasaki, M., Martin-Puig, S., Sun, Y., Evans, S. M., Laugwitz, K.-L., and Chien, K. R. (2006) Multipotent embryonic isl1+ progenitor cells lead to cardiac, smooth muscle, and endothelial cell diversification. *Cell* **127,** 1151–1165
64. Niu, Z., Yu, W., Zhang, S. X., Barron, M., Belaguli, N. S., Schneider, M. D., Parmacek, M., Nordheim, A., and Schwartz, R. J. (2005) Conditional mutagenesis of the murine serum response factor gene blocks cardiogenesis and the transcription of downstream gene targets. *J. Biol. Chem.* **280,** 32531–32538
65. Boucher, P., Gotthardt, M., Li, W.-P., Anderson, R. G. W., and Herz, J. (2003) LRP: role in vascular wall integrity and protection from atherosclerosis. *Science* **300,** 329–332
66. Adrain, C., and Freeman, M. (2012) New lives for old: evolution of pseudoenzyme function illustrated by iRhoms. *Nat. Rev. Mol. Cell Biol.* **13,** 489–498
67. Sun, Z., Feng, D., Fang, B., Mullican, S. E., You, S.-H., Lim, H.-W., Everett, L. J., Nabel, C. S., Li, Y., Selvakumaran, V., Won, K.-J., and Lazar, M. A. (2013) Deacetylase-independent function of HDAC3 in transcription and metabolism requires nuclear receptor corepressor. *Mol. Cell* **52,** 769–782
68. Neeb, Z., Lajiness, J. D., Bolanis, E., and Conway, S. J. (2013) Cardiac outflow tract anomalies. *Wiley Interdiscip. Rev. Dev. Biol.* **2,** 499–530
69. Singh, N., Trivedi, C. M., Lu, M., Mullican, S. E., Lazar, M. A., and Epstein, J. A. (2011) Histone deacetylase 3 regulates smooth muscle differentiation in neural crest cells and development of the cardiac outflow tract. *Circ. Res.* **109,** 1240–1249
70. Bajolle, F., Zaffran, S., Meilhac, S. M., Dandonneau, M., Chang, T., Kelly, R. G., and Buckingham, M. E. (2008) Myocardium at the base of the aorta and pulmonary trunk is prefigured in the outflow tract of the heart and in subdomains of the second heart field. *Dev. Biol.* **313,** 25–34
71. Tao, G., Kotick, J. D., and Lincoln, J. (2012) Heart valve development, maintenance, and disease: the role of endothelial cells. *Curr. Top. Dev. Biol.* **100,** 203–232
72. Loeys, B. L., Schwarze, U., Holm, T., Callewaert, B. L., Thomas, G. H., Pannu, H., De Backer, J. F., Oswald, G. L., Symoens, S., Manouvrier, S., Roberts, A. E., Faravelli, F., Greco, M. A., Pyeritz, R. E., Milewicz, D. M., Coucke, P. J., Cameron, D. E., Braverman, A. C., Byers, P. H., De Paepe, A. M., and Dietz, H. C. (2006) Aneurysm syndromes caused by mutations in the TGF-β receptor. *N. Engl. J. Med.* **355,** 788–798
73. Yasuda, H., Nakatani, S., Stugaard, M., Tsujita-Kuroda, Y., Bando, K., Kobayashi, J., Yamagishi, M., Kitakaze, M., Kitamura, S., and Miyatake, K. (2003) Failure to prevent progressive dilation of ascending aorta by aortic valve replacement in patients with bicuspid aortic valve: comparison with tricuspid aortic valve. *Circulation* **108,** II291–II294
74. Gordon, K. J., and Blobe, G. C. (2008) Role of transforming growth factor-beta superfamily signaling pathways in human disease. *Biochim. Biophys. Acta* **1782,** 197–228
75. Lahm, A., Paolini, C., Pallaoro, M., Nardi, M. C., Jones, P., Neddermann, P., Sambucini, S., Bottomley, M. J., Lo Surdo, P., Carfí, A., Koch, U., De Francesco, R., Steinkühler, C., and Gallinari, P. (2007) Unraveling the hidden catalytic activity of vertebrate class IIa histone deacetylases. *Proc. Natl. Acad. Sci. U.S.A.* **104,** 17335–17340
76. Potthoff, M. J., and Olson, E. N. (2007) *MEF2 and HDAC Proteins Regulate Striated Muscle Development and Remodeling*. Ph.D thesis, University of Texas Southwestern Medical Center, Dallas, TX
77. Piera-Velazquez, S., Li, Z., and Jimenez, S. A. (2011) Role of endothelial-mesenchymal transition (EndoMT) in the pathogenesis of fibrotic disorders. *Am. J. Pathol.* **179,** 1074–1080
78. Chen, T., and Dent, S. Y. R. (2014) Chromatin modifiers and remodellers: regulators of cellular differentiation. *Nat. Rev. Genet.* **15,** 93–106
79. Margueron, R., and Reinberg, D. (2011) The Polycomb complex PRC2 and its mark in life. *Nature* **469,** 343–349